Journal of the European Ceramic Society 42 (2022) 2230–2247

Contents lists available at ScienceDirect

Journal of the European Ceramic Society

journal homepage: www.elsevier.com/locate/jeurceramsoc

Phase coexistence and grain size effects on the functional properties of $BaTiO_3$ ceramics

V.A. Lukacs [a], M. Airimioaei [a,b], L. Padurariu [a], L.P. Curecheriu [a], C.E. Ciomaga [a,c], A. Bencan [d], G. Drazic [e], M. Avakian [f], J.L. Jones [f], G. Stoian [g], M. Deluca [h], R. Brunner [h], A. Rotaru [i], L. Mitoseriu [a,*]

[a] Dielectrics, Ferroelectrics & Multiferroics Group, Faculty of Physics, Al. I. Cuza University of Iasi, 11 Carol I Blvd., 700506, Iasi, Romania
[b] Faculty of Chemistry, Al. I. Cuza University of Iasi, 11 Carol I Blvd., 700506, Iasi, Romania
[c] Department of Exact and Natural Sciences, Institute of Interdisciplinary Research, Al. I. Cuza University of Iasi, 11 Carol I Blvd., 700506, Iasi, Romania
[d] Electronic Ceramics Department, Jožef Stefan Institute, Ljubljana, 1000, Slovenia
[e] Department of Materials Chemistry, National Institute of Chemistry, 1000, Ljubljana, Slovenia
[f] Department of Materials Science & Engineering, North Carolina State University, Raleigh, NC, 27695, USA
[g] National Institute of Research and Development for Technical Physics, 700050, Iasi, Romania
[h] Materials Center Leoben Forschung GmbH, Roseggerstraße 12, A-8700, Leoben, Austria
[i] Faculty of Electrical Engineering and Computer Science & MANSiD Research Center, Stefan cel Mare University, 13 Universitatii St., 720229, Suceava, Romania

ARTICLE INFO

Dedicated to the memory of Paolo Nanni.

Keywords:
$BaTiO_3$
Size effects
Phase superposition
Dielectric properties

ABSTRACT

The functional properties of a series of $BaTiO_3$ ceramics, having grain sizes ranging from 75 nm to 2.25 μm, with polymorph coexistence around room temperature are presented. Large temperature ranges of phase coexistence were detected through structural analyses, with no apparent size effect on the extension of co-existence domain, while the transition temperatures vary with grain size. Permittivity values are among the highest reported and the typical maximum around 1 μm grain size is confirmed by low field measurements and sub-switching Rayleigh analysis. An interesting feature not reported elsewhere is the persistence of permittivity maximum above Curie temperature and under high dc field at saturation, where domain walls contribution is minimal, raising questions about the largely accepted interpretation concerning the domain walls role on permittivity maximum. The planar defects in the starting powders give rise to extended strained defects in the ceramics, impacting their functional properties and multi-phase character.

1. Introduction and theoretical aspects

The studies concerning scale- and size-dependent properties of ferroelectrics are among the most important and long-lasting research topics aimed to clarify the role of size reduction on the functional properties of materials and resolve questions the stability of ferroelectric long-range order at small sizes. The downscaling has a huge impact in modern electronics, which are subjected to a continuous trend of miniaturization, thus forcing the feature sizes of electronic components and devices to shrink accordingly [1,2]. Extensive studies concerning scale-dependent phenomena were dedicated to a large number of ferroelectric compounds, and in particular to $BaTiO_3$, the most important ferroelectric oxide employed mostly in passive components [3,4]. Although in the past decades the research mostly involved the modification of properties when reducing grain size at submicronic levels (below 150−200 nm) in polycrystalline $BaTiO_3$ ceramics [5–9], the interest shifted recently again on the intermediate domain of grain size (comprising 1−2 μm range) [10–15].

Grain size reduction substantially suppresses functional properties such as dielectric permittivity, piezo- and pyroelectric coefficients, polarization, and nonlinear dielectric character (tunability) with respect to the bulk $BaTiO_3$ ceramics values [3,4]. The large majority of material constants show a strong decay when reducing grain size below 500 nm [3–9], while in the intermediate range of sizes ~(1−2) μm, maximum room temperature values of a few important properties like piezo-, pyro- and dielectric constants were observed, regardless the raw materials, synthesis procedure and sintering methods used to produce $BaTiO_3$ polycrystalline ceramics [3,4,10–15]. The position of permittivity and

* Corresponding author.
E-mail address: lmtsr@uaic.ro (L. Mitoseriu).

https://doi.org/10.1016/j.jeurceramsoc.2021.12.024
Received 20 September 2021; Received in revised form 20 November 2021; Accepted 9 December 2021
Available online 10 December 2021

piezoelectric coefficient d_{33} maxima and the corresponding values of material constants are slightly scattered in literature, in particular for d_{33} and this was explained by considering variations of internal stress, purity, Ba/Ti stoichiometry, density or defects induced by the employed precursors and processing methods [4]. Nevertheless, the existence of a limited range of grain size, *i.e.* a "critical size" around 1 μm for which the ceramics show enhanced properties, is a generally accepted universal behaviour for $BaTiO_3$ ceramics. Understanding the microstructural origin for enhanced properties in order to design $BaTiO_3$ ceramics with superior properties for applications is the major reason of the renewal interest in this grain size range, besides the curiosity-driven fundamental aspects originating such behaviour, which are still under discussion in the scientific community. The origin of permittivity and piezoelectric coefficients maxima was intensely debated by various authors in terms of internal stresses producing peculiar domain structures (twinning) causing an increase of intrinsic contributions [16–19], or in terms of extrinsic domain wall movement contributions, *i.e.* to a maximization of 90 ° domain wall density and/or mobility in the range of critical size [12,13,20–23].

At high temperature, $BaTiO_3$ is nonpolar (paraelectric) with a cubic (C) $Pm\bar{3}m$ perovskite structure. It becomes polar (ferroelectric) below the Curie temperature (near $120\,^{\circ}C < T_C < 128\,^{\circ}C$) with a $P4mm$ tetragonal (T) distortion. Further cooling below temperatures of about $5\,^{\circ}C < T_{O\text{-}T} < 10\,^{\circ}C$, a structural transformation occurs into an $Amm2$ orthorhombic (O) state, which turns into a rhombohedral $R3m$ polymorph at even lower temperatures near $-90\,^{\circ}C < T_{R\text{-}O} < -80\,^{\circ}C$. These phase transformations are first order type, with thermal hysteresis and they are accompanied by anomalies of physical properties and material constants. The reduction of grain size in sub-micron range induces a decrease of T-C phase transition (Curie) temperature and a slight increase of the O-T and R-O transition temperatures, together with a reduction of material constants and broadening of the property *vs.* temperature dependences [3–68,24–27]. This trend was also predicted by the calculations of Lin *et al.* [28] based on Landau theory, through the following expansion of the free energy:

$$\begin{aligned} G = {} & \alpha_1\left(P_1^2+P_2^2+P_3^2\right)+\alpha_{11}\left(P_1^4+P_2^4+P_3^4\right)+\alpha_{12}\left(P_1^2P_2^2+P_1^2P_3^2+P_2^2P_3^2\right) \\ & +\alpha_{111}\left(P_1^6+P_2^6+P_3^6\right)+\alpha_{112}\left[P_1^2\left(P_2^4+P_3^4\right)+P_2^2\left(P_1^4+P_3^4\right)+P_3^2\left(P_1^4\right.\right. \\ & \left.\left.+P_2^4\right)\right]+\alpha_{123}P_1^2P_2^2P_3^2+\alpha_{1111}\left(P_1^8+P_2^8+P_3^8\right)+\alpha_{1112}\left[P_1^6\left(P_2^2+P_3^2\right)\right. \\ & \left.+P_2^6\left(P_1^2+P_3^2\right)+P_3^6\left(P_1^2+P_2^2\right)\right]+\alpha_{1122}\left(P_1^4P_2^4+P_1^4P_3^4+P_2^4P_3^4\right) \\ & +\alpha_{1123}\left(P_1^6P_2^2P_3^2+P_2^6P_1^2P_3^2+P_3^6P_1^2P_2^2\right), \end{aligned} \tag{1}$$

where P_1, P_2 and P_3 are the components of the polarization along the crystallographic axis and α parameters were proposed as constants, irrespective of grain size (*GS*) and temperature (*t*), excepting α_1 and α_{12} which were considered as size dependent:

$$\alpha_1 = \alpha_{10}(t - t_C) + K_1/GS \tag{2}$$

where α_{10} and K_1 are constants, t_C is the Curie temperature and:

$$\alpha_{12} = \alpha_{12}' + K_2/GS \tag{3}$$

where α_{12}' and K_2 are constants.

The expression for the free energy, Eq. (1), proposed in Ref. [28] represents a development from the approach used by Li *et al.* [29] for single-crystals, by including the increasing influence of shear stresses when reducing grain size. All the numerical values for the α and K parameters can be found in the original work of Lin *et al.* [28] The Landau-based common approach to derive the phase polymorphs at a given temperature is to find the absolute minima of Gibbs free energy for different values of the polarization components (P_1, P_2 and P_3). Generally, the minimum free energy corresponds to the following cases: (i) $P_1 = P_2 = P_3 \neq 0$ (R polymorph), (ii) $P_1 = P_2 \neq 0$, $P_3 = 0$ and the analogous cases (O polymorph), (iii) $P_1 \neq 0$, $P_2 = P_3 = 0$ and the analogous cases (T phase), and (iv) $P_1 = P_2 = P_3 = 0$ (C phase). Several representations of the free energy for different orientations of polarizations with respect to P_1, P_2 and P_3 axis are shown in Fig. 1 for coarse and fine grain sizes (10 μm *vs.* 100 nm) at a few significant temperatures (−59 °C, 13 °C and 100 °C). All the points on the selected surfaces in Fig. 1 represent free energy minima positions for different orientations of polarization.

Fig. 1 comparatively shows that, at the same temperature of −59 °C, in a coarse-grained ceramic [Fig. 1(a)] the minimum free energy is established in the O phase (blue colour), while in a fine-grained ceramic [Fig. 1(d)], the minimum free energy corresponds to the R polymorph. Similarly, at a temperature of 13 °C, a coarse ceramic [Fig. 1(b)] presents a minimum value for the free energy in T phase, while a fine ceramic [Fig. 1(e)] in its O phase. At higher temperatures (100 °C), both kinds of ceramics [Fig. 1(c) and (f)] are characterized by a well-defined and stable minimum of free energy in the T phase. The usual approach to derive phase diagrams in ferroelectrics by using Landau theory is to identify the absolute minimum of free energy and the corresponding phase polymorph. This simplification leads to sharp phase transitions characterized by continuous and narrow lines in the phase diagram. For example, the three black lines represented in Fig. 2 are identical with those computed by Lin et al. [28] and they correspond to grain sizes and temperatures characterized by the same free energy minimum for two distinct phases. However, the free energy representations from Fig. 1 show that in the range of phase transitions more than one polymorph in a stable free energy minimum may be found. For example, a ceramic with grain size of 10 μm [Fig. 1(b)] is characterized by an absolute free energy minimum in the T phase, but the O polymorph is also described by a local stable equilibrium. In a similar way, the ceramic with grain size of 100 nm has a stable free energy minimum in the T phase, although the free energy value corresponding to the O state is lower. At lower temperatures (−59 °C), both O and R phases are stable irrespective of ceramic grain sizes, as shown in Fig. 1(a) and (d). The fact that in specific temperature ranges at least two polymorphs may be present with different weights explains thermal hysteresis behaviour in first-order phase transformations.

These representations indicate that for complex $BaTiO_3$ ceramic systems containing a large number of grains, particularly considering the innate grain size distributions that occur in real materials, the structural phase transitions may be not sharp. Most likely, the transition between polymorphs is realized in a wide range of temperatures. In order to qualitatively describe the phase concentrations at different temperatures, a Monte Carlo procedure was employed, similarly as proposed by Horchidan *et al.* [30] The algorithm, based on the principle of the energy minimization, starts from a random value and orientation of a single-grain polarization and it consists of successive and small modifications of polarization. These modifications are accepted if they lead to a decrease of the Gibbs free energy (similar to a Metropolis algorithm). The calculations are stopped when a stable free energy minimum is reached, with polarization and energy that are stable with respect to ones corresponding to previous steps. Once the stable energy minimum is reached, the corresponding phase polymorph is firstly identified for a single grain. Then, the procedure is repeated for 10000 grains in order to statistically derive the concentrations of polymorphs for a given GS and temperature.

According to these calculations, the phase diagram (Fig. 2) shows that, for coarse ceramics ($GS > 10\,\mu m$), the transition between the minimum values of the free energy corresponding to the R and O phases occurs at −71 °C, while the R and O phases coexist in a range of temperatures from −108 °C to−33 °C. Similarly, the O – T transition takes place between −33 °C and 35 °C and the T-C transition occurs in the temperatures range of (115 °C, 130 °C). The temperature domains corresponding to these polymorph transformations become narrow when reducing GS down to 10 nm, and the average transition temperatures (R-O, O-T and T-C) suffer modifications similar to the experimentally ones

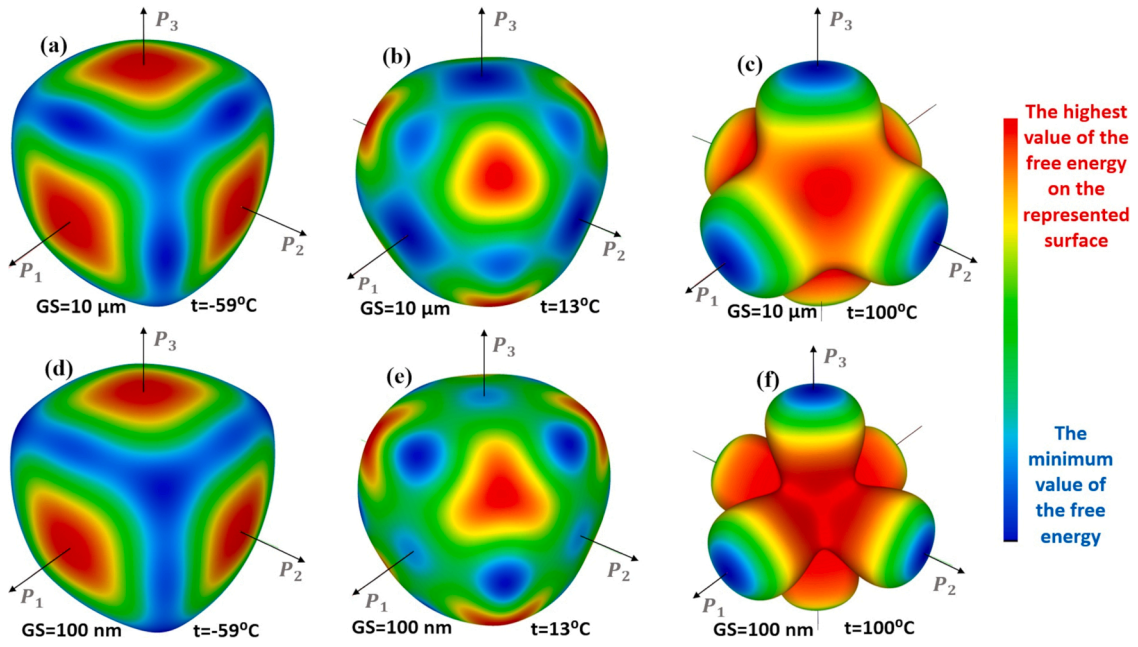

Fig. 1. Representation of surfaces corresponding to the free energy minimum positions for different orientations (components) of polarization vectors for coarse (GS = 10 µm) and fine (GS = 100 nm) grains. The free energy value on these surfaces is represented in colour scale.

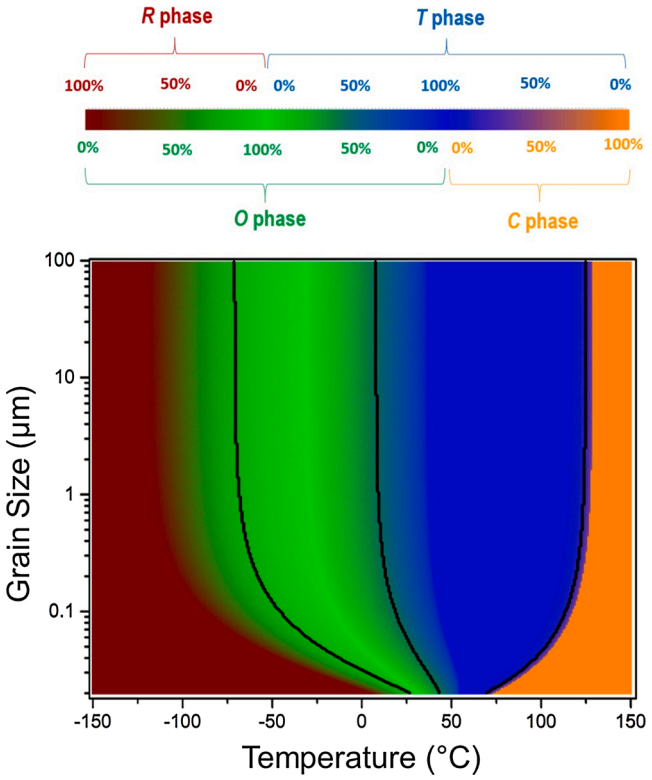

Fig. 2. Generalized *Grain size - temperature* phase diagram in $BaTiO_3$ ceramics computed from Landau-based theory. The weights of the Rhombohedral (R), Orthorhombic (O), Tetragonal (T) and Cubic (C) polymorphs are represented in colour scale and the black lines are characterized by the same free energy minimum in two phases.

collected from literature in Ref. [27] (Fig. 3). Therefore, the *grain size - temperature* phase diagram predicts that for any GS, there is a temperature range of polymorph phases coexistence in $BaTiO_3$. For example, O and T symmetries may coexist around room temperature for any grain

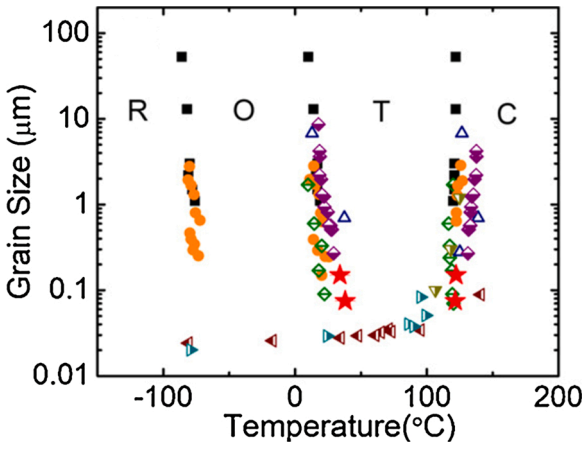

Fig. 3. Generalized *Grain size - temperature* phase diagram in $BaTiO_3$ ceramics derived from experimental data (data collected and figure adapted from Ref. [27]). Polymorphs are denoted as: R (rhombohedral), O (orthorhombic), T (tetragonal) and C (cubic).

sizes, while for very small grain sizes, below 100 nm, all the polymorphs with variable amounts may coexist.

In the studies concerning size-dependent properties of polycrystalline $BaTiO_3$ ceramics, including recent comprehensive reviews [3,4,31], the possible role of phase superposition was not considered, with exception of some investigations relating the crystallographic structure of $BaTiO_3$ to their piezoelectric performances [32]. The co-existence of polymorphs may have an important role in enhancing functional properties, as found in $BaTiO_3$-based solid solutions at morphotropic phase boundaries [30,33,34]. Additionally, the material constants determined after subjecting the samples to high dc fields (poling), *e.g.* piezo-, pyroelectric and electrocaloric coefficients or dc-tunability (permittivity *vs.* dc field) may be affected, since the applied field may modify the weights of co-existing polymorphs or even induce new phases in a reversible or irreversible way [12,24].

In the present paper, BT ceramics with variable GS in the (75–2250) nm range showing phase superposition close to the room temperature

have been investigated in order to check how their structural and functional properties are affected by their GS reduction.

2. Materials and methods

Hydrothermally synthesized $BaTiO_3$ nanopowders (Sigma Aldrich, purity: ≥ 99 %) with average particle size of ~60 nm, with cubic symmetry, $Pm\bar{3}m$, were employed to produce dense ceramics with variable grain size by using a two-step sintering method (Fig. S1, Supplementary material). In the first step, the nanopowders were consolidated by Spark Plasma Sintering (SPS Model FCT-(FAST) HPD5) at 950 °C for a short sintering time of 3 min. under a pressure of 70 MPa. Further, selected pellets were subjected to a pressureless sintering step, after SPS, at progressively increasing temperatures in the range of (950–1250) °C for 1 h, to induce a controlled grain growth. In this way, ceramics produced from the same powder, with variable grain size in the range of 75 nm to 2.25 μm and densities in the range of 93 %–98 % were obtained. All the sintered ceramics were subjected to a re-oxidation annealing for 36 h, followed by a slow cooling down to the room temperature in order to reduce the high concentration of oxygen vacancies that usually contribute to the total dielectric response, remove the carbon contamination and relieve the possible residual stresses.

The ceramic micro/nanostructures were examined by using a Cross Beam System - Carl Zeiss NEON 40EsB scanning electron microscope (SEM). Samples for scanning transmission electron microscopy (STEM) were prepared by a combination of mechanical polishing, followed by argon ion beam milling to electron transparency. The grain size (GS) values were assessed through measurements with ImageJ open source (Image Processing & Analysis Software) on the surface SEM micrographs and the average value was calculated as arithmetic mean by considering ~200 grains. STEM studies were carried out using a Cs-corrected Jeol ARM 200 CF STEM probe operated at 200 kV, equipped with Jeol Centurio EDXS system and a Gatan Quantum ER Dual Electron Energy Loss Spectroscopy (EELS) system.

The phase purity of powders and ceramics was checked by X-Ray diffraction with a Shimadzu LabX 6000 diffractometer using Ni-filtered Cu-Kα radiation (λ = 1.5418 Å) with scan step increments of 0.02 ° and counting time of 1 s/step, for 2θ ranged between (20 °–80 °). The crystalline structure was determined by Rietveld refinement carried out using the General Structure Analysis System (GSAS) software package, developed by Larson & Von Dreele [35]. Variable temperature diffractograms were collected with a PANalytical Empyrean diffractometer under *in-situ* heating/cooling, in the range of (−20, 180) °C, with a 2θ step of 0.013 °, at a rate of 2 °C/scan. Multi-peak fitting procedure was employed to determine the peak position and full width at half maximum (FWHM) intensity values aimed for monitoring the temperature-induced structural changes.

Raman Spectroscopy was performed on all sets of samples with a LabRAM 300 (Horiba Jobin Yvon, France) with 532 nm laser excitation and 1800 g/mm grating. Measurements were done in the range of (−196, 196) °C (slightly varied), with steps of 10 °C, to see the full range of phase transitions, using a Linkam THMS 600 temperature stage. Raman spectra were plotted in the Origin 9.0 software after correcting for the Bose-Einstein population factor (using Wolfram Mathematica software). The peak fitting program Labspec 4.0 from Horiba Jobin Yvon was employed to determine the phase transition temperatures.

For the electrical characterization, the ceramic pellets were polished and electroded with silver paste and then measured in parallel plate capacitor configuration by impedance spectroscopy with an Agilent E4980 bridge and Solartron 4284A impedance analyser, at temperatures of (0, 180) °C and frequency range of (1 Hz, 1 MHz). The high voltage dc-tunability measurements were performed at room temperature on the ceramic disks immersed in transformer oil. The ceramics were subjected to high dc voltages (with a maximum applied dc field of 25 kV/cm) produced by a function generator coupled with a TREK 30/20A-H-CE amplifier (Trek Inc., Medina, NY) [36] while being tested by using a LCR - 8105 G (GW Instek, New Taipei City, Taiwan) under ac low field of 10 V/cm at various frequencies, in order to determine the permittivity and tangent loss *vs.* dc field. The room temperature macroscopic hysteresis P(E) loops were recorded on ceramics placed in silicon oil by using a modified Sawyer-Tower circuit fed by a sinusoidal waveform with an amplitude of E = 25 kV/cm and at a testing frequency of 10 Hz produced by a function generator (DS345, Stanford Res. Systems, Sunnyvale, California) coupled with a High-Voltage Amplifier (Trek 609E-6, Trek Inc., Medina, NY). Rayleigh subswitching loops were determined under the same conditions by using variable field amplitudes below the coercive field.

Differential scanning calorimetry (DSC) analysis was performed in the range of (-20, 150) °C with a DSC 8000 – Differential Scanning Calorimeter (PerkinElmer Inc.). The transition temperature was estimated from the peak position of the absorbed heat and the heat of transition was obtained from the area of the DSC peaks.

3. Results and discussions

3.1. Microstructural and structural analysis

After the consolidation by SPS, pellets with a relative density of ~88−90% and homogeneous microstructure with equiaxed grains have been produced [Fig. 4(a)].

The obtained average grain size of ~75 nm indicates that, during the SPS process, the grain growth was limited and only a few larger grains in the range of 120−150 nm are observed in some regions. Further sintering for 1 h at progressively increasing temperatures (T_{sint}) from 950 °C to 1200 °C promoted a homogeneous grain growth up to the final average grain size values of: 275 nm (T_{sint} = 950 °C), 450 nm (T_{sint} = 1050 °C), 735 nm (T_{sint} = 1100 °C), 1100 nm (T_{sint} = 1125 °C), 1500 nm (T_{sint} = 1150 °C) and 2250 nm (T_{sint} = 1200 °C), respectively. All ceramics show faceted equiaxed grains and relative densities in the range of 93–98 %. Therefore, by using this method, a set of homogeneous ceramics covering a large range of grain sizes, produced from the same powders, can be compared.

Room temperature (20 °C) X-ray diffraction patterns obtained from the fractured surfaces of $BaTiO_3$ ceramics, with various grain sizes from 75 nm to 2250 nm are shown in Fig. 5. The nanopowders were indexed with $Pm\bar{3}m$ cubic symmetry (Fiche 01-074-1963) with unit cell parameter a = 4.0243 Å. After the SPS consolidation, a broadening of the peak (s) near the region in which the tetragonal 002 and 200 reflections should appear is observed in the diffractogram for the finest ceramic (75 nm), indicating a reduced spontaneous strain for a tetragonal-like polar structure. By increasing the sintering temperature, a sharpening of peaks and increase of splitting as result of grain growth is noticed, together with an inversion of the I_{002}/I_{200} peak intensities ratio with respect to one corresponding to the finest ceramics. The I_{002}/I_{200} ratio determined from the experimental patterns of polycrystalline tetragonal piezoceramics is usually about ~0.58, close to the multiplicity ratio of 0.50 characterizing ceramics with randomly oriented domains [37–39]. Modifications of this intensity ratio may be related to the surface texturing (preferential domain orientation) induced by dc-field poling or by mechanical stress [40–42], but it can also be an indication of the presence of other polymorphs than tetragonal (like orthorhombic O state), or of possible phase superpositions [32]. With the exception of the ceramic with 75 nm grain size, which has the highest porosity level, of ~12 %, all the other $BaTiO_3$ ceramics show a ratio $I_{002}/I_{200} > 1$. Their patterns cannot be fitted with a single tetragonal phase. Rietveld refinement (example of fits shown in Fig. S2, *Supplementary material*) indicates the presence of a mixture of O and T phases, with an amount of T phase in the range of (49–52)% and a rise of tetragonal spontaneous strain c/a when increasing grain size, from ~1.0065 (75 nm) to ~1.0100 (1500 nm). It should be mentioned that the XRD patterns for the present

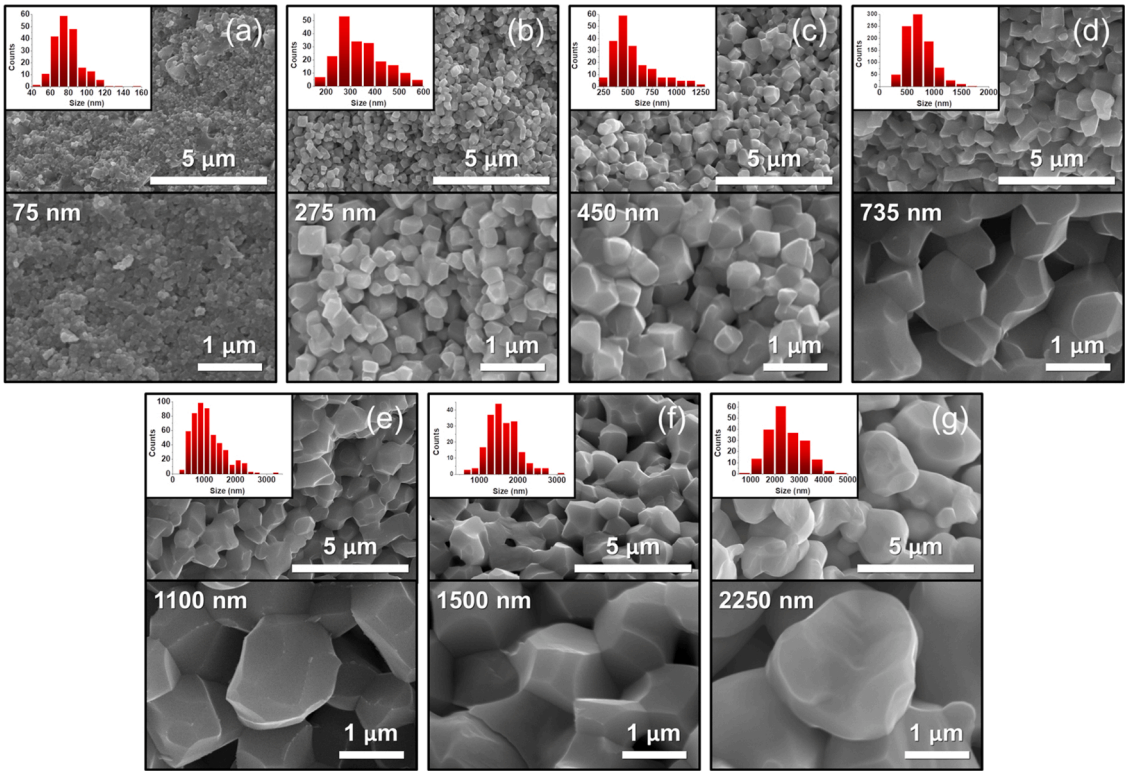

Fig. 4. SEM micrographs of the $BaTiO_3$ ceramics with various grain sizes: 75 nm (a), 275 nm (b), 450 nm (c), 735 nm (d), 1100 nm (e), 1500 nm (f), and 2250 nm (g) collected in fresh fractured surfaces. Inset: corresponding grain size distribution.

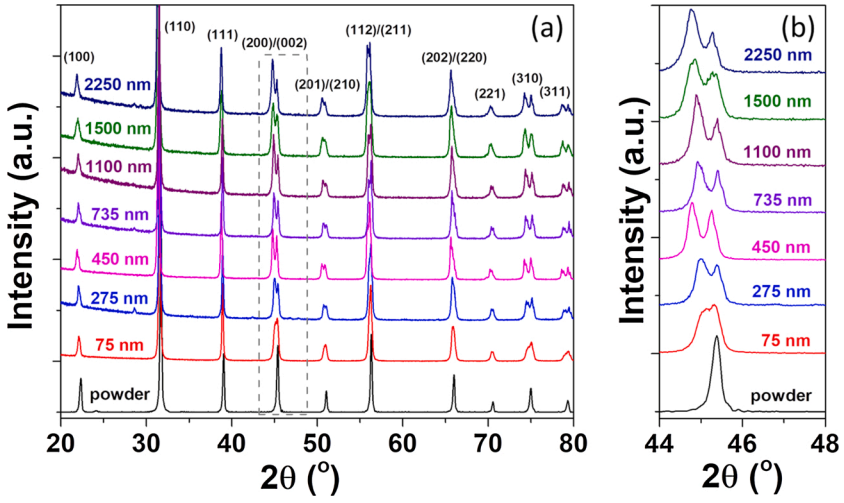

Fig. 5. X-Ray diffraction patterns of $BaTiO_3$ ceramics with different GSs (a). Magnified representation of peaks in the region in which the tetragonal 002 and 200 peaks appear (b).

study were recorded from the ceramic surfaces after the post-sintering re-oxidation treatment and the ceramics have not been subjected to cutting or polishing prior to the experiment, because such processing may produce texturing near the surface due to the ferroelastic nature of 90 ° domain walls, as reported for PZT [37] or $BaTiO_3$ [39] ceramics. Therefore, the multi-phase structural character of the present set of ceramics seems to be related to an intrinsic volume effect and not to a surface one. It is worthwhile to note that the tendency towards O state expected from Landau calculations when reducing GS seems to be not observed in the present XRD patterns for the finest ceramic (~75 nm), but one should also consider the high level of porosity in the ceramics purely subjected to SPS without subsequent pressureless sintering with respect to the ones that were subjected to a subsequent pressureless sintering step. In any case, the phase coexistence can be inferred for all the GSs at room temperature, but for a precise determination of phase amounts higher resolution structural analysis would be necessary.

Although $BaTiO_3$ is usually T at room temperature, O phase or intrinsic structural instability were also reported in literature: ceramics prepared from different types of powders, consolidated by various methods and characterized by various ranges of grain sizes and densities also demonstrated phase superposition at room temperature. For example, ultrafine $BaTiO_3$ dense ceramics with GS ~ 30 nm present phase superposition with O (33.7 %) and T (66.3 %) weights [43], while ceramics synthesized *via* SPS with grain size above 300 nm were not

purely T [44]. Coarse ceramics sintered by classical sintering from powders produced by solid state [32,45], or hydrothermally synthesized [32] present a structural modification from T to O polymorph (with ranges of phase coexistence), when raising the sintering temperature from 1160 °C to 1180 °C. Even for $BaTiO_3$ single crystals analysed with high resolution structural methods there are still debates concerning the room temperature polymorphs: it was reported as strictly T in Ref. [46], while a monoclinic transitional state between the T and O phases was demonstrated in Ref [47]. or intrinsic instability with monoclinic and O states within a majority T phase [48]. By detailed nanoscale local structural analyses it was recently found that high-quality crystals present nanoscale symmetry fluctuations, *i.e.* regions of a few tens of nanometres retaining almost perfect symmetry are interspersed in regions of lower symmetry [49]. In ceramics, such fluctuations may be stabilized at larger scale by defects, internal fields or stress. Therefore, due to the variations related to the specific synthesis and consolidation methods determining particle and ceramic grain size, shape, distribution and internal defects or porosity, we may expect variations of polymorph phase composition in $BaTiO_3$ ceramics or the presence of other symmetries together with T at room temperature, which is close to the O-T phase transformation nominal range.

We further investigated if grain size plays any role on the phase superposition and on its extension during the temperature-induced phase transformations in this set of ceramics. Four samples with grain size of 75 nm, 450 nm, 1100 nm (around the critical grain size with expected high permittivity values) and 2250 nm were selected for the temperature-dependent XRD study. Fig. 6 shows the modifications induced by temperature in the XRD patterns near the scattering angle at which the perovskite cubic 002 reflection appears. Since we do not draw conclusions about phase stability directly from the raw XRD data, we refer to the collection of peaks measured in this range as the 002_{PC} region, where PC refers to a pseudo-cubic reference frame. The 002_{PC} region of $BaTiO_3$ ceramics as a function of grain size and temperature are also shown as 3D surface plots in Fig. S3 of *Supplementary material*.

By using a multipeak fitting procedure (*e.g.*, as shown in Fig. S4, *Supplementary material*), the temperature dependences of the peaks in the 002_{PC} region across the O – T – C structural transformations were determined as a function of GS (Fig. 7). For all the grain sizes, large temperature ranges of phase coexistence are indicated by the presence of multi-peak features around room temperature and no apparent grain size effect on the extension of phase co-existence range can be precisely determined.

Below 10 °C, all the diffraction patterns show features characteristic to O polymorph. By increasing the temperature, the symmetry turns into T, as detected by the modification of the peak positions and inversion of I_{002}/I_{200} ratio. The T symmetry detected for temperatures in the range of (30–120) °C for grain sizes GS = 450 nm, 1100 nm and 2250 nm transforms into a C state at ~120 °C, where the peaks within the 002_{PC} region merge into a single peak [Fig. 7(b)–(d)].

The peak splitting in the 002_{PC} region is very small for the ceramic with GS = 75 nm above 10 °C and due to this, no apparent ferroelectric-paraelectric transformation can be detected in Figs. 6(a) and 7 (a). This is consistent with the lowest spontaneous strain determined in the finest ceramic (*i.e.* essentially existing in a pseudo-cubic state). However, even with peaks in the 002_{PC} region potentially being highly overlapping, the change in profile shape with temperature (*e.g.*, as measured by the full width at half maximum, FWHM) can suggest changes in phase constitution [43]. In the present work, the existence of a broad ferroelectric-paraelectric structural transformation between room temperature and ~120 °C is confirmed by a gradual reduction of FWHM ratio of the highly overlapping tetragonal 002 and 200 reflections with respect to the constant value of 111 reflection *vs.* temperature for the ceramic with GS = 75 nm (Fig. S5, *Supplementary material*).

3.2. Raman analysis

To better assess the peculiarities of the structural transitions as a function of GS, to check for the T symmetry in the finest ceramic (GS = 75 nm) and confirm the temperature ranges for the phase superposition as a function of GS at a lower length scale, Raman spectroscopy was employed in all investigated materials.

Fig. 8 reports the Bose-Einstein-corrected and normalized Raman spectra collected on $BaTiO_3$ ceramics with various GSs in a temperature range from −194 °C to 196 °C. The precise temperature intervals we used are indicated in the figure; generally, a 10 °C step was used. The structural transitions are detected as following: (i) R-O transformation is marked by a decrease in intensity to zero by the peak at ~170 cm^{-1} [Fig. 8(a)] [50]; (ii) O-T transition can be seen by the disappearance of

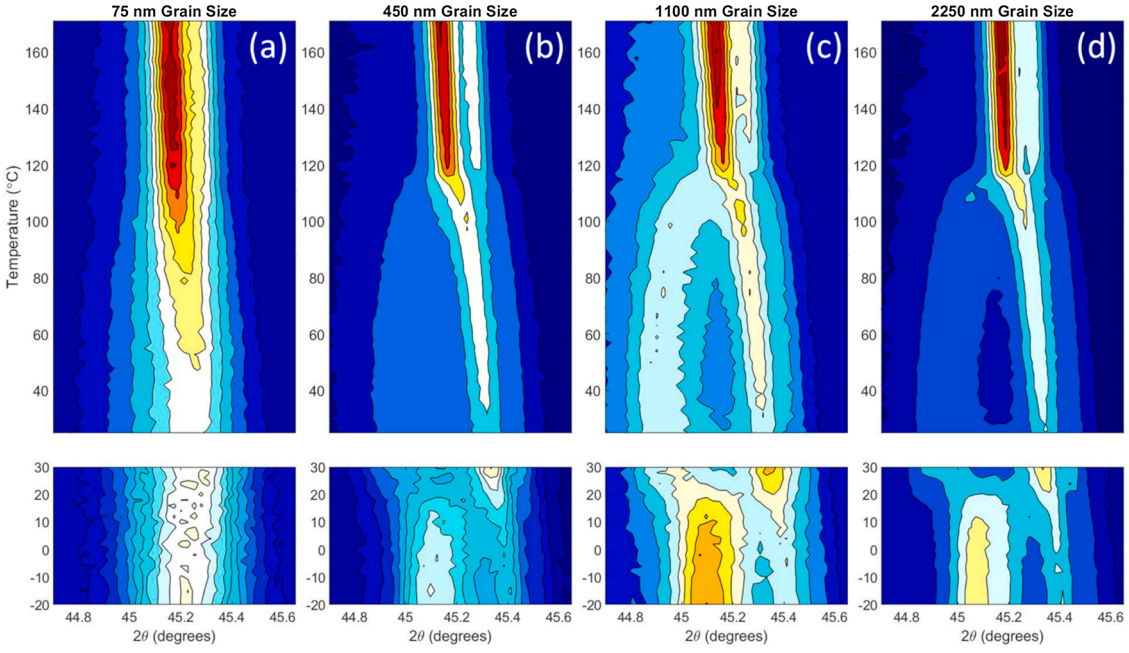

Fig. 6. Contour plots of changes in intensities near the 002_{PC} region *vs.* temperature in the range of O-T and T-C structural phase transformations of $BaTiO_3$ ceramics with variable grain sizes: 75 nm (a), 450 nm (b), 1100 nm (c), and 2250 nm (d).

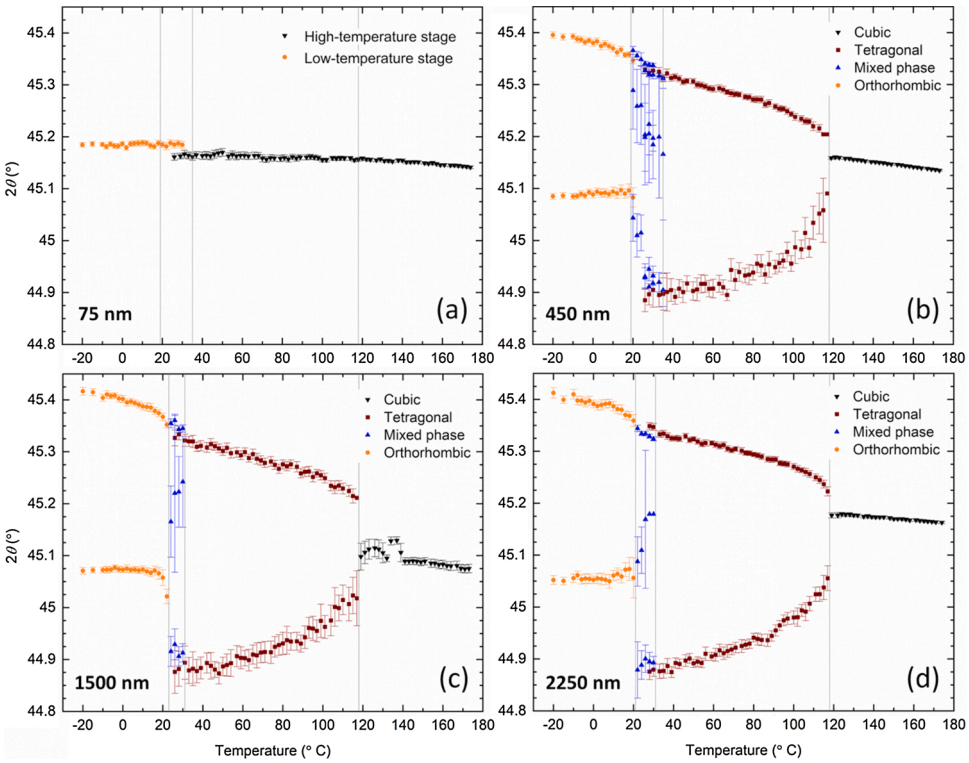

Fig. 7. Temperature dependence of peak positions in the 002_{PC} region of $BaTiO_3$ ceramics with variable GSs: 75 nm (a), 450 nm (b), 1100 nm (c), and 2250 nm (d).

the 190 cm^{-1} peak, and the concurrent appearance of an interference dip at 180 cm^{-1} [51,52] [Fig. 8(b)] and (iii) the Curie temperature is seen in the disappearance of the ~305 cm^{-1} peak and a significant change in the overall shape of the Raman spectra. In the cubic phase, in fact, only two broad features are seen, centred at ~270 cm^{-1} and ~525 cm^{-1}. In finer samples, the 305 cm^{-1} peak does not completely disappear, suggesting that ferroelectric distortion is still present (in those samples) also at temperatures above the corresponding Curie temperature. The 305 cm^{-1} mode, in fact, is responsible for vibrations involving Ti and O atoms in a unit cell where Ti is in an off-centre position [53]. This mode is persistent up to the maximum measured temperature of 196 °C in both the 75 nm and 450 nm samples, and up to at least 176 °C in the 1.1 μm ceramic, indicating that the existing local polar distortion is very stable up to elevated temperatures, higher than the expected macroscopic Curie temperature of bulk $BaTiO_3$ ceramics [44]. In the 2.25 μm sample, this peak disappears above 126 °C, which is compatible with the Curie temperature of traditional $BaTiO_3$ ceramics. Hence, there is a general downward trend in the transition temperatures, which seem to be decreasing with GS increase. This stabilization of the polar phase at high temperature is most probably a short-range effect, given the sensitivity of Raman measurements down to the unit cell scale, and is likely mediated by the strain introduced in the lattice by GS reduction and by possible structural defects. Interestingly, the strain related with the finer GS seems to stabilize also the orthorhombic phase much above room temperature. This can be seen in the 75 nm sample by the persistence of the 190 cm^{-1} peak up to the maximum recorded temperature (196 °C), as this mode was ascribed to strain-driven orthorhombic phase stabilization in nanosized $BaTiO_3$ ceramics [54]. Hence, in the sample with the smallest GS, the local structure stays orthorhombic up to above the Curie temperature of regular bulk $BaTiO_3$ ceramics. Although it cannot be excluded that also tetragonal phase is present at high temperatures, the presence of the orthorhombic phase is unambiguously confirmed. Considering the length scale sensitivity difference between the two techniques, the Raman analysis confirms the multi-phase character around room temperature observed by temperature-dependent XRD analysis, where even the finest ceramic was found to have the smallest tetragonal spontaneous strain at room temperature and the 002/200 splitting and O-T and T-C transitions were almost not detectable by temperature-dependent structural analysis [Fig. 8(a)].

A multi-phase character is also likely in the coarser ceramics. In all other samples [Fig. 8(b)–(d)], the 190 cm^{-1} peak persists up to 16 °C, but the tetragonal dip at 180 cm^{-1} is evident also for lower temperatures, and a shift of the 270 cm^{-1} mode at higher temperatures (~36 °C for all samples) could also be related to the O-T transition [50]. Polar distortion (in this case tetragonal) is present up to 196 °C in the 450 nm sample, up to 176 °C in the 1.1 μm sample, and up to 126 °C in the 2.25 μm sample.

The presence of a polar (O) distortion far above T_c at a length scale below the coherence length of laboratory XRD (~20 unit cells) suggests that, in spite of its high porosity level (12 %) with respect to the other samples, the finest ceramic (75 nm) is most probably subjected to a higher internal stress resulted from the fast SPS consolidation, which was not fully relaxed even after the re-oxidation thermal treatment. As discussed in Ref. [4], densification by SPS, which occurs in conditions very far from equilibrium, may provide in the final ceramic different levels of defects (as type and concentrations) than in samples consolidated by conventional sintering. The role of surface effects related to the high weight of grain boundaries with respect to the ceramic bulk (volume effect) may also play a role in this behaviour.

In the larger grain samples (GS ≥ 450 nm), there is no major change in the Raman spectrum (compared to traditional $BaTiO_3$) concerning the O-T transition, but local strain possible related to structural defects may still be present at short range due to the persistence of polar (T) distortions up to 196 °C in the 450 nm sample and up to 176 °C in the 1.1 μm sample. The detected ranges for the structural transition temperatures by Raman analysis as a function of grain size are indicated in Table S1, Supplementary material.

3.3. Low field dielectric properties

3.3.1. Variation of permittivity with grain size

Low field permittivity *vs.* temperature for the series of $BaTiO_3$ ceramics with different GSs, at a few selected frequencies in the (10^2, 10^6)

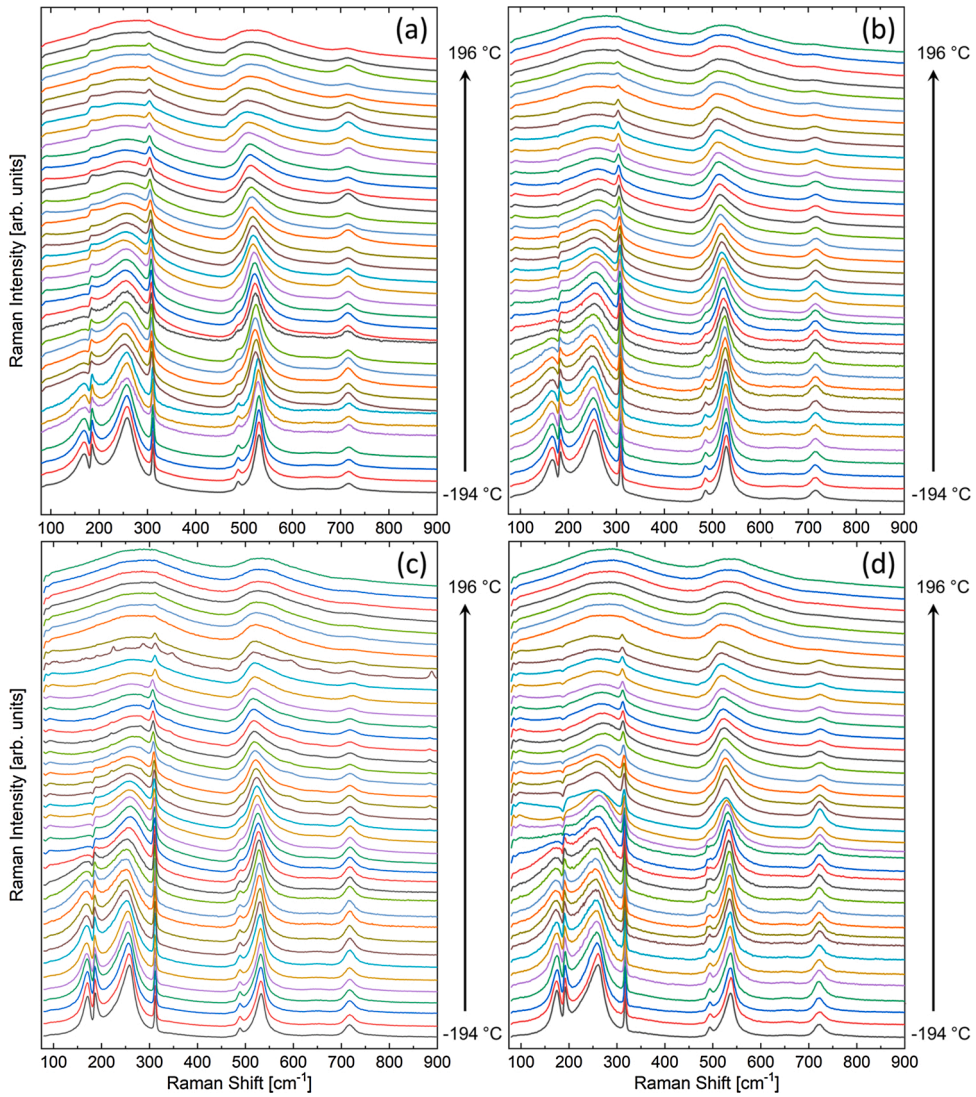

Fig. 8. Raman spectra in dependence of temperature for $BaTiO_3$ ceramics with variable GSs: 75 nm (a), 450 nm (b), 1100 nm (c), and 2250 nm (d).

Hz range are presented in Fig. 9(a)–(g). These dependences show well-defined anomalies assigned to the structural phase transformations: a small maximum around room temperature of ~20 °C (O-T) and a pronounced peak at Curie temperature T_C, at about ~120 °C (T-C). These transition temperatures show opposite trends when reducing GS: O-T range increases, while the T-C temperature decreases at smaller GS.

The corresponding critical temperatures as revealed by the permittivity *vs.* temperature data [Fig. 9(h)–(i)], temperature dependent XRD and Raman analyses were completed with results from differential calorimetry data (shown in Fig. S6, *Supplementary material*) and are plotted as a function of GS in Fig. 10. The obtained experimental phase diagram shown in Fig. 10 confirms that all the investigated $BaTiO_3$ ceramics are at room temperature in the range of phase superposition and indicates the tendency of reduction for the T-C and increasing of O-T temperatures when reducing GS, as predicted by Landau calculations (Fig. 2), and are similar to experimental data obtained by other authors (Fig. 3). Additionally, Raman analysis indicated that at short range order level, the finer the grains were, the higher than the macroscopic Curie range were the temperatures at which they maintained their local polar character.

The corresponding dielectric losses are below 6% for all the ceramics. A small frequency dispersion is present below T_C and a stronger dispersion indicated by a permittivity increase at small frequencies and high temperatures (above 140 °C) is found only for larger GS (>735 nm) [Fig. 9(d)–(g)]. For inducing grain growth in the $BaTiO_3$ nanoceramics after SPS, progressively higher temperatures were employed during the presureless sintering step. Due to this, a larger amount of oxygen vacancies most probably resulted at higher temperature and they were not completely removed during the post-sintering reoxidation step, thus generating a thermally-activated Maxwell-Wagner extrinsic response at low frequencies [13,55]. At high frequency (*e.g.* 10 kHz), such effects become negligible and a comparison between permittivity as a function of GS can be derived for all the series of ceramics [Fig. 9(h)]. The decay of Curie (T_C) and Curie-Weiss (T_0) temperatures provided by Curie-Weiss analysis when reducing GS are observed in Fig. 9(i). The faster decay of T_0 with respect to Curie temperature (T_C) *vs.* GS in $BaTiO_3$ ceramics was usually interpreted in literature as determined by a "dilution" effect, related to the increasing role of non-ferroelectric grain boundaries when reducing GS down to nanoscale [6,8,56–60]. For the present ceramics, the Curie temperature revealed by permittivity *vs.* temperature data increases from 114 °C for the ceramic with GS of 75 nm and saturates to 120 °C for GS above 1000 nm, similar to other values reported in literature [3,4], as shown in Fig. 11(a).

The permittivity measured at room temperature (25 °C) for f = 10 kHz shows maximum values of about 4500–4700 for ceramics with GS in the range of ~1000 nm, corresponding to the general trend of permittivity *vs.* GS collected from literature data [Fig. 11(b)]. The permittivity maximum around 1 μm in $BaTiO_3$ ceramics was previously

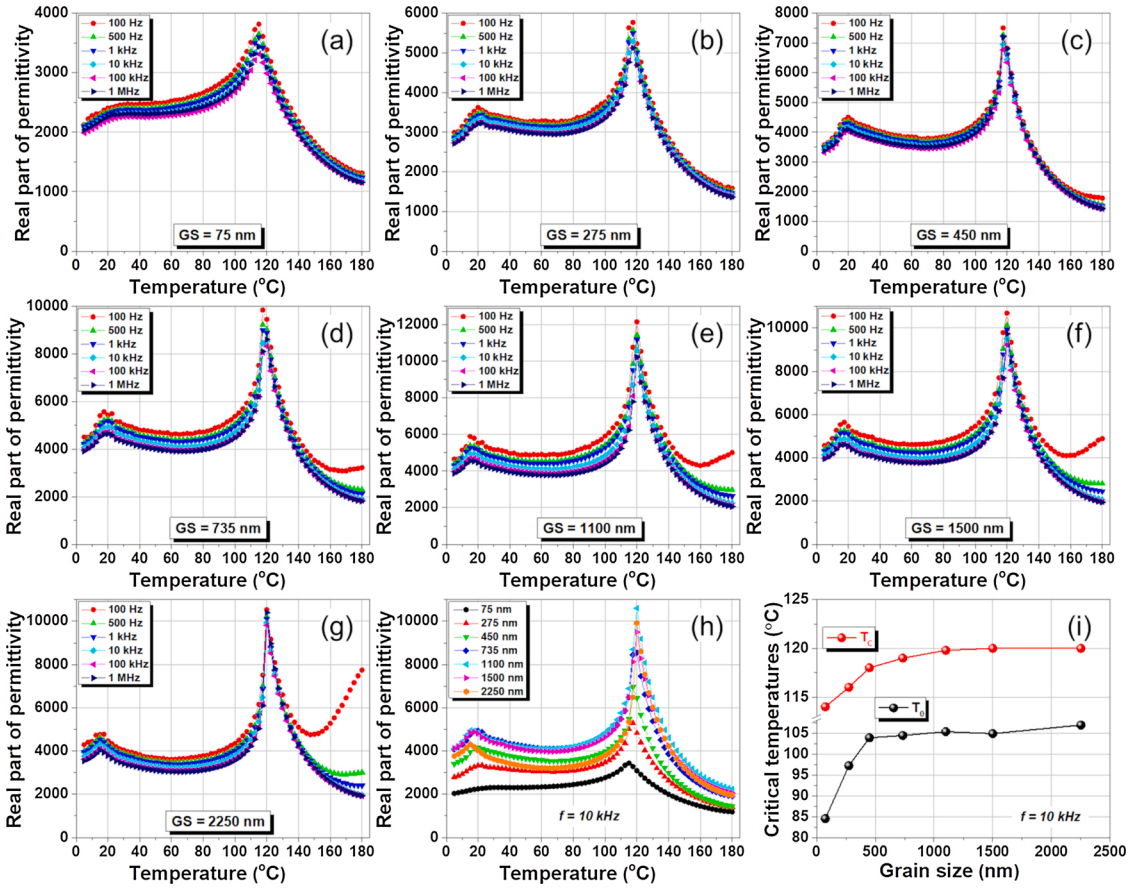

Fig. 9. Real part of permittivity *vs.* temperature (a-g) of $BaTiO_3$ ceramics with various grain sizes in the (75–2250) nm range, at a few selected frequencies. Comparison showing the role of grain sizes on the temperature dependence of permittivity determined at f = 10 kHz (h). Grain size dependence of Curie and Curie-Weiss temperatures, determined for f = 10 kHz (i).

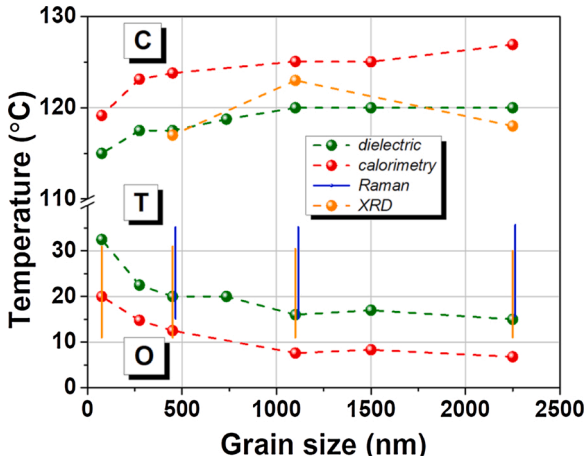

Fig. 10. Experimental grain size – temperature phase diagram in $BaTiO_3$ ceramics. Bars indicate the temperature ranges of O-T structural transformations as detected from XRD and Raman experiments.

discussed either in relationship with internal residual stress contributions [18,61] or in terms of maximized domain density [20,62] or enhanced 90° domain wall mobility [12], giving rise to superior extrinsic contributions to the permittivity and piezoelectric coefficients. For all the range of GSs, the permittivity of the present series of ceramics is higher than that obtained in our previous studies for similar GSs [6,8]. In particular, a remarkable high value, ~2350, is observed for the finest ceramic of 75 nm (which is among the highest reported for such grain size in $BaTiO_3$ ceramics), in spite of its lower density, of 88 %. This result can be related to the observed phase superposition around room temperature for all the GSs (*i.e.* due to the proximity of O-T phase transformation). High permittivity in fine ceramics can be also related to cleaner and thinner non-ferroelectric grain boundaries in the fine ceramics, thus limiting the "dilution effect" of permittivity with respect to other studies for similar GSs [4,6,44,56–58,63].

3.3.2. *Rayleigh analysis (sub-switching properties)*

Further insights concerning the permittivity contributions can be extracted by using Rayleigh analysis of the non-linear dielectric responses under sub-switching fields, which enables separation of the role of reversible (intrinsic lattice contribution and reversible extrinsic contributions) and irreversible extrinsic components as a function of GS. Such analysis was scarcely performed in relation with GSs. The extrinsic contribution is mainly produced by the response of field-induced movement of domain walls, but mobile defects, interfaces, interphase boundaries, *etc.* may also give a contribution to the overall response. The Rayleigh law, originally proposed for ferromagnetic materials, describes the interaction of domain walls moving on a randomly varying force with lattice defects (vacancies or other charged defects, dislocations, interfaces, *etc.*) acting as pinning centres [74–78]. When domain walls are trapped by pinning defects, they can "jump" to other pinning centres if the electric field is high enough to overcome a threshold field E_{th} which is much lower than the coercive field able to induce polarization switching. This is an irreversible process which modifies the overall polarization, since the domain walls cannot return exactly to their initial positions after field removal. If the driving force is lower than the threshold field, the domain walls may vibrate harmonically around their

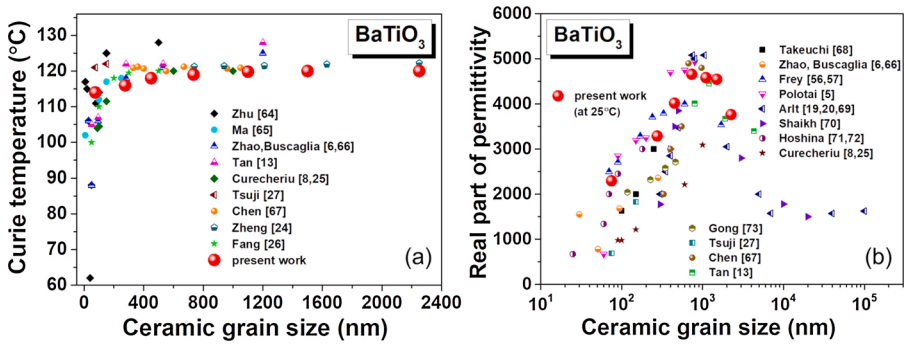

Fig. 11. Ceramic grain size dependence of Curie temperature (a) and real part of permittivity measured at room temperature (b) (data collected from literature [5,6,8,13,19,20,24–2756,57,64–73] and present work).

equilibrium position and the corresponding response is fully reversible. Therefore, in sub-switching conditions, besides the intrinsic lattice contribution, both reversible and irreversible domain wall movement are contributing to the dielectric response and permittivity follows a linear dependence *vs.* field amplitude (Rayleigh law): $\varepsilon = \varepsilon_{in} + aE_0$, where ε_{in} is the linear permittivity (at zero field amplitude) determined by lattice deformation (intrinsic component) and reversible domain wall vibrations. Therefore, ε_{in} is related to non-hysteretic reversible processes only and it was associated to a measure of domain wall mobility [78,79], while ε is the permittivity under the applied field with E_0 amplitude and contains both reversible and irreversible contributions. The term aE_0, where a is the non-linear Rayleigh coefficient, describes the sub-switching hysteretic response, *i.e.* the extrinsic effect induced by the irreversible domain wall motion.

For the present set of ceramics, the measured polarization under increasing ac-field amplitude indicates a higher threshold field E_{th} for inducing the onset of measurable dielectric nonlinearity when reducing GS, from 2.5 kV/cm for GS ≥ 1500 nm to about 15−20 kV/cm for GS ≤ 275 nm, similar to the trend reported in Ref. [80]. The analysis of sub-switching P(E) loops within the Rayleigh framework reveals an interesting dependence upon GS (Fig. 12). The zero-field intrinsic permittivity increases from relative values of 2083 for GS = 75 nm to a maximum of ~4125 for GS = 1000 nm and then drops to ~3000 for GS ≥ 1500 nm, all of permittivity values being slightly lower than ones determined from low-field dielectric measurements. Therefore, the permittivity maximum in the critical range of ~1000 nm is also confirmed by the ε_{in} *vs.* GS dependence [Fig. 12(a)] and indicates a drop of domain wall mobility, for GSs below 1000 nm as well as for GS ≥ 1500 nm, in $BaTiO_3$ ceramics. The non-linear Rayleigh coefficient a [Fig. 12(b)] presents a fast rise when increasing GS up to 500 nm, followed by a monotonous increase with a tendency to saturation for GS ≥ 1500 nm. Data concerning the ratio of the irreversible to reversible Rayleigh parameters for the dielectric response of a variety of bulk and thin film ferroelectrics were reported in literature [81]. As a general trend, it was observed that this ratio is about one order in magnitude smaller for hard compositions with respect to the soft PZT ceramic compositions, while for a given composition, films were harder than their ceramic counterparts, having even a lower a/ε_{in} ratio. This feature was interpreted as being related to the higher defect concentration, clamping due to the film substrate and finer grain size in films than in ceramics, all of them yielding a lower concentration of movable domain walls and of other mobile interfaces, which resulted in a lowering of extrinsic contributions to the permittivity and piezoelectric coefficients. However, no reports concerning the size effects on Rayleigh parameters were published in literature to date, with exception of Ref. [82] in which it was shown that the nonlinear domain wall contribution to the d_{33} piezoelectric coefficient in coarse $BaTiO_3$ ceramics was much larger (up to 35 %) with respect to ones determined in finer ceramics. For the present samples, the ratio between the nonlinear and linear contributions to the dielectric response aE_0/ε_{in} (at a given field of 6 kV/cm) reaches ~19−20 % for GS ≥ 1500 nm and strongly decreases with one order of magnitude to about ~2% for the finest ceramic (GS = 75 nm). A study concerning scaling effects for PZT films with columnar grains reports a strong decay of the a/ε_{in} ratio when reducing film thickness [83], which shows similar features as the decay obtained in Fig. 12(c) when reducing GS and similar Rayleigh coefficient values. Therefore, the decay observed in the a/ε_{in} *vs.* GS dependence seems to be a general trend of a scale-dependent property. Besides a reduction in domain wall density towards the single-domain regime, the increasing amount of grain boundaries when reducing ceramic GS at the nanoscale would increase the clamping of domain walls, thus making their field-induced movement increasingly more difficult, both in sub-switching regime and at high fields, and for ultrafine GS a frozen-like domain structure poorly responsive to the applied field is ultimately reached [66]. The fact that no anomalies related to the irreversible contributions in a and a/ε_{in} *vs.* GS dependences [Fig. 12(b)–(c)] are observed around the critical GS ~ 1000 nm lead us to conclude that mostly the intrinsic and reversible domain wall contributions are responsible for the well-defined maximum of both low-field permittivity and ε_{in} determined from the Rayleigh analysis. This feature is in agreement with the results reported in Ref. [12], where it was shown that around the critical size corresponding to the permittivity maximum, a maximum 90 ° domain wall

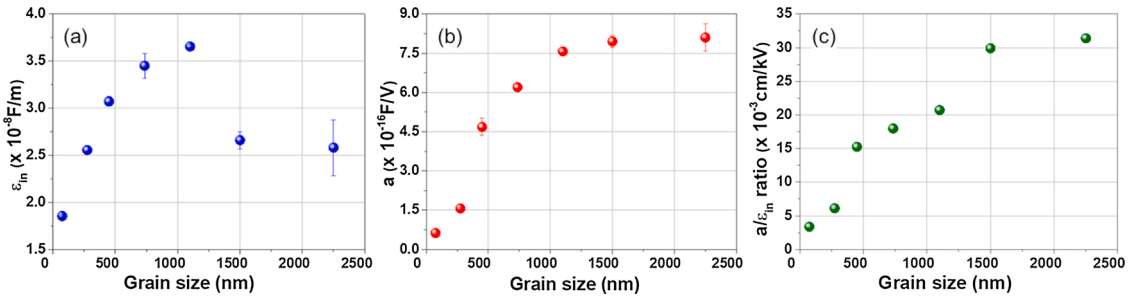

Fig. 12. Grain size dependence of linear dielectric permittivity ε_{in} (a), Rayleigh coefficient a (b), and their ratio ε_{in}/a (c) for $BaTiO_3$ ceramics.

mobility was detected both at low and high fields and also with the observations of enhanced intrinsic dielectric contribution (maximum of ε_{in}) around the Curie temperature or in the compositional range of MPB reported in Refs. [34,82], where domain wall mobility was also enhanced. It is worthwhile to note that multi-phase behaviour around room temperature for all the GSs in the present $BaTiO_3$ ceramics may favour enhancement of domain wall movement with respect to other types of $BaTiO_3$ ceramics reported earlier. This fact explains the overall large permittivity values obtained in the present study with respect to previous ones [Fig. 11(b)]. However, no relevant specific structural features with possible impact on the critical behaviour in the range of GS ~ 1000 nm could be accurately determined.

3.4. Grain size influence on the high field nonlinear properties

3.4.1. Polarization vs. field loops

Polarization *vs.* field P(E) loops recorded in ac dynamic regime [Fig. 13(a)] show regular size dependent switching properties, with a tendency of polarization and loop area reduction when diminishing GS while preserving quite similar coercive fields, ranging between 7.5 kV/cm and 9 kV/cm [Fig. 13(b)]. With respect to other reports, the present polarization values are rather low for GSs above 500 nm [10,13,39] and slightly higher than ones reported in Ref. [84], while the finest ceramics show well-defined non-linear loops with polarization similar as observed in Ref. [85], but with higher polarization than reported in Refs [25,86,87]. for similar GSs.

Usually the reduction of switching character towards a behaviour specific to linear dielectrics [25,66] is considered mainly caused by the grain boundary clamping effect on domain walls, which strongly limits domain reorientation and switching when reducing GS at nanoscale towards the single domain regime, but an intrinsic effect determined by the reduction of long-range dipolar contribution is not excluded. In spite of these contributions, the switching with well-defined *P(E)* loops for smaller GS in the present set of $BaTiO_3$ ceramics may be related to the observed phase coexistence around room temperature, giving rise to a higher domain wall mobility as well as to more possibilities for the polarization orientation than in ceramics with purely tetragonal state.

A monotonic reduction of spontaneous and remanent polarization when reducing GS from coarse to nanostructured ceramics is expected as result of continuous reduction of tetragonality when reducing GS [4]. Such a dependence was reported for $BaTiO_3$ ceramics prepared by spark plasma sintering, but also a polarization diminishing for larger GS, above 1 μm, was observed for samples produced by classical sintering, as presented in Ref. [13]. In that study, the *P(E)* loops are quite similar for GS ≥ 500 nm, with a slightly higher value of remanent polarization for GS = 1100 nm [Fig. 13(b)], followed by a reduction at larger GS. Literature data scarcely describe macroscopic *P(E)* loops as a function of GS in $BaTiO_3$ ceramics and no systematical trend was reported, as found for the $\varepsilon(GS)$ dependence. A higher value of switching/remanent polarization around GS ~ 1 μm, where also the permittivity and d_{33} show their maximum values, was found in stoichiometric $BaTiO_3$ ceramics and in ones with a slight Ba excess [14], while in Ref [84]. a polarization maximum was determined at GS ~ 3 μm for ceramics prepared by classical methods, while their piezoelectric coefficient shows a maximum value around GS ~ 1 μm. In fact, the ferroelectric P(E) loops and their corresponding characteristics (saturation and remanent polarization, coercive field, loop area) are dependent on various factors, such as microstructure (GS, porosity, grain boundaries), mechanical stress, structural symmetry, charged defects, *etc.* For the present samples, a slight reduction of polarization for larger GS (above 1 μm) may be caused by pinning domain walls by the oxygen vacancies, which were suggested by the low field dielectric data to be present in larger amounts for coarser ceramics.

3.4.2. Permittivity vs. field dependence (dc-tunability) and field-induced structural transformations

As prepared, ceramics show a non-linear permittivity *vs.* applied dc field dependence [Fig. S7(a)–(d), *Supplementary material* and described in detail in the *Supplementary material: Tunability analysis and discussion on field-induced structural modifications*), with a small hysteresis for all the GSs and with some anomalies at intermediate fields of (5–10) kV/cm, which were not reported in other previous works concerning single-phase $BaTiO_3$ ceramics [8,25]. Such peculiar features are possibly related to the coexistence of polymorphs around room temperature observed in the present study. In systems with metastable states, field-induced structural transformations are likely and they may be the origin of such anomaly in the $\varepsilon_r(E)$ dependences, or in field-induced increase of strain [45], as well as the existence of a threshold field necessary to unpin domain walls trapped in some deep defect energy levels. With respect to data reported in Ref. [12], where polymorphic field-induced transformation was detected by using in-situ field cycling during the structural analysis in coarse ceramics only, here such behaviour is expected for much finer ceramics, starting with GS ≥ 275 nm, from the $\varepsilon_r(E)$ anomalies. The observed anomalies were completely reproducible after cycling the dc field in the ±30 kV/cm range, various times at room temperature. Structural analysis performed on such ceramics in remanence (after being subjected to a room temperature poling field, then removed) qualitatively indicated field-induced modifications of O-T amounts (described in detail in *Supplementary material*), which are compatible with Landau-based calculations [30]. Therefore, one might conclude that the present $BaTiO_3$ ceramics are not in a full equilibrium state after processing and reversible field-induced structural modifications are likely during the tunability experiments.

The ceramics were stabilized after performing a stronger depolarization refreshment by using two thermal heating/cooling cycles at 600 °C with an intermediate field-induced depolarization step by using ac cycling fields with f = 10 Hz, with decreasing amplitude from the maximum value of ±40 kV/cm to zero. After this kind of depolarization, the equilibrium tunability characteristics and shape of the $\varepsilon_r(E)$ de-

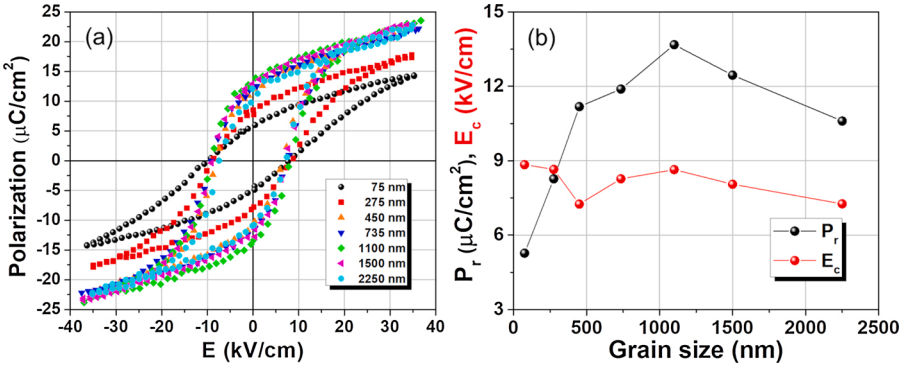

Fig. 13. P(E) hysteresis loops (a) and the dependence of remanent polarization and coercive field (b) *vs.* grain size in $BaTiO_3$ ceramics.

pendences were slightly modified with respect to ones characteristic to the as-prepared ceramics and they remained fully reproducible after various heating/cooling cycles at 600 °C or after the application of dc field cycles with amplitudes in the ±30 kV/cm range, at room temperature. Therefore, these tunability characteristics can be considered as representative to describe the equilibrium response of $BaTiO_3$ ceramics under high dc fields.

The corresponding $\varepsilon_r(E)$ dependences for the refreshed ceramics presented in Fig. 14(a)–(g) do not show any visible anomalies at intermediate fields. A well-defined hysteretic behaviour is noticed for all the GSs, with a tendency for saturation above 15 kV/cm for larger GS and a decreasing coercive field when increasing GS. Unlike the other ceramics, the finest one, with GS = 75 nm [Fig. 14(a)], has a small variation below 10 kV/cm, followed by a faster decrease of permittivity at higher fields (at 20 kV/cm permittivity decreased ~1.5 times with respect to its zero-field value), and without reaching saturation, as result of a combined effect of low GS and lower density. It is worthwhile to note that denser $BaTiO_3$ nanoceramics investigated in our previous studies were characterized by a much lower tunability, *e.g.* a field-induced permittivity decrease of about ~1.1 times for GS = 150 nm [63] and of ~1.03 for GS = 90 nm [25] with respect to their zero field values, under similar dc field with amplitude of 20 KV/cm. In the previous studies, the lowering of tunability and permittivity was described as related to the progressive increasing role of non-ferroelectric low-permittivity grain boundaries when reducing GS to nanoscale [8,25]. However, the present $BaTiO_3$ nanoceramics show both higher permittivity and tunability, which may be related to the polymorphs superposition around room temperature allowing a higher domain wall mobility, to clean grain boundaries, and to extrinsic contributions from nanopolar regions. As indicated by the Raman results, such nanopolar regions are very stable up to higher temperatures, the finer the grains (from 136 °C for GS = 2.25 μm to above 196 °C for GS = 75 nm, see Table S1 in the Supplementary material).

The comparison between permittivity *vs.* dc field dependences at various GSs shown in Fig. 14(h) reveals an interesting fact about the saturation permittivity and raises some questions about the features related to the critical GS ~ 1 μm in $BaTiO_3$ ceramics, as it will be discussed in the next paragraph.

4. Discussions concerning the critical behaviour of permittivity around 1 μm

Room temperature permittivity *vs.* GS determined at various dc field amplitudes at field increase/decrease (Fig. 15) shows that in the range of critical size, of ~1100 nm, not only the low field permittivity (*i.e.* one determined at $E_{dc} = 0$) presents a maximum, but this trend is maintained when applying dc fields up to the maximum available one, of 25 kV/cm, close to the saturation. Moreover, if at zero and small dc fields, the permittivity maximum *vs.* GS is flat and covers a broad GS range of ~ (700, 1500) nm, the maximum becomes better defined and sharper around ~1100 nm, when the permittivity is measured during the application of high dc fields. This trend is clearly observed also in Fig. 14 (h) and was never observed previously. Reports concerning poling effects on the GS dependence of permittivity are scarce, with the exception of Ref. [24], where a reduction of permittivity with about 25 % in the range of critical GS ~ 940 nm, was measured after poling tetragonal $BaTiO_3$ ceramics under a very high dc field of 50 kV/cm at ~105 °C. In that paper, the maximum of permittivity at GS ~ 940 nm in the poled ceramics (measured in remanence) seems to be still maintained, although there are no data below 740 nm to confirm such a trend. It is worthwhile to note that present results (Figs. 14 and 15), in which permittivity decreases with more than 50 % under $E_{dc} = 25$ kV/cm for GS = 1100 nm were collected under the applied dc field and not in remanence after poling, as in Ref. [24].

The fact that literature data concerning piezoelectric coefficients d_{33} as a function of GS (which is always determined after the ceramic was subjected to dc fields for poling and then measured in remanence conditions) evidenced anomalies in the same range of GSs [13,14,24], indicates the existence of common mechanisms responsible for the scaling effects of dielectric and piezoelectric properties at ultra-low and at high fields around the critical GS ~ 1 μm. These features were assigned to extrinsic contributions related to a higher domain wall density and domain wall mobility specific to $BaTiO_3$ ceramics in the range of critical GS, in particular at low and moderate fields [12,13]. However, a decreasing complexity of the domain configuration is expected in $BaTiO_3$ ceramics when applying high dc fields and a tendency towards a single-domain state for saturation, when the domain wall density is minimized. The single domain state can rarely be reached even in high purity single-crystals under high fields, because the multidomain state is favoured for its low electrostatic energy even though no mechanical constraints are present on the crystal surfaces [88]. Moreover, in polycrystalline ceramics, grains are mechanically confined and single-domain state is hardly reachable by poling even at ultrahigh fields, because of high internal stresses from the incompatible transformation strain at grain boundaries and inhomogeneous electric fields related to the anisotropy of permittivity [24,89]. Under high dc poling fields, most probably small existing domains are strongly spatially confined, located at grain boundaries, on charged or structural defects or

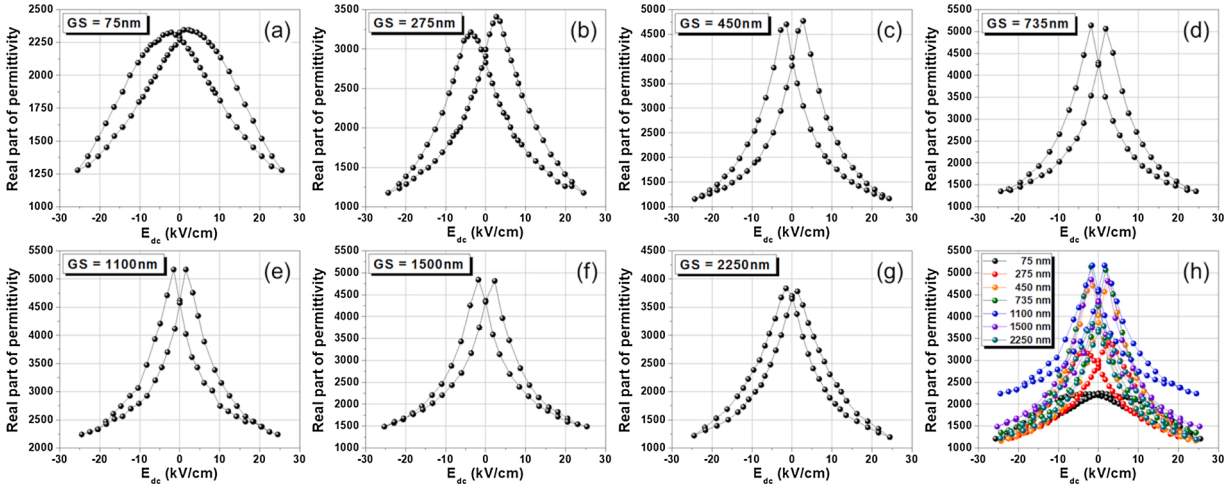

Fig. 14. Permittivity *vs.* dc field dependences for each grain size indicated in the corresponding figure [(a)–(g)] and their comparative behaviour at various grain sizes (h).

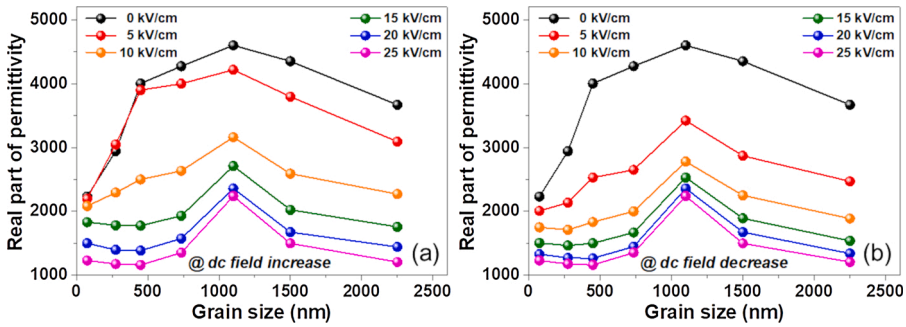

Fig. 15. Grain size dependence of dielectric constant measured at various dc field amplitudes indicated in figures at field increase (a) and field decrease (b) cycles.

at interphase boundaries are still present and their reversible movement under small ac excitation may contribute to the dielectric response. A very recent study [90] revealed the existence of static polar nanoclusters of 2−4 nm size and low symmetry in the nominally nonpolar cubic phase of $BaTiO_3$ at 200 °C. Such polar regions were interpreted as originating from local strain variations and their field-induced modifications determine the material's properties in the paraelectric state. For the present set of ceramics, the existence of nanopolar regions at high temperatures in the average cubic state was suggested by the existence of Raman activity above the Curie range. Their stability up to high temperatures was enhanced in finer ceramics as result of suggested increasing internal stresses when reducing GS, and not around 1 μm. For some reason not well understood yet, these extrinsic contributions are also enhanced around the critical size of 1 μm, as ones due to the ferroelectric domain wall mobility reported in other works [12]. The role of phase coexistence around room temperature and possible field-induced structural transformations in the ceramic volume may also play a role in the observed features.

In addition, the domain wall contribution is expected to be progressively eliminated by heating above the Curie temperature, when ceramics are subjected to their ferroelectric-paraelectric phase transition. The low-field permittivity determined as a function of GS at various temperatures (data collected from Fig. 9) indicates a reduction of permittivity above the Curie temperature following the Curie-Weiss behaviour, while the permittivity maximum at GS = 1100 nm is preserved even at 150 °C and at 180 °C (Fig. 16). When increasing temperature, the domain structure tends to disappear at the ferroelectric-paraelectric transition, *i.e.* the domains progressively reduce in size and confine into smaller volume (nanopolar regions) within a cubic matrix and they survive far away from the Curie temperature, as shown by Raman analysis. Therefore, even if the ferroelectric domain wall contributions should be eliminated in the paraelectric state, the existence of mobile nanopolar regions as well as of other interphase boundaries or defects, showing enhanced mobility around the critical GS ~ 1 μm, may contribute to maintaining a dielectric maximum in $BaTiO_3$ ceramics, even in the absence of large-scale ferroelectric domains. There are no other reports for permittivity as a function of GS in paraelectric state of $BaTiO_3$ ceramics with variable GS to compare with the present observations.

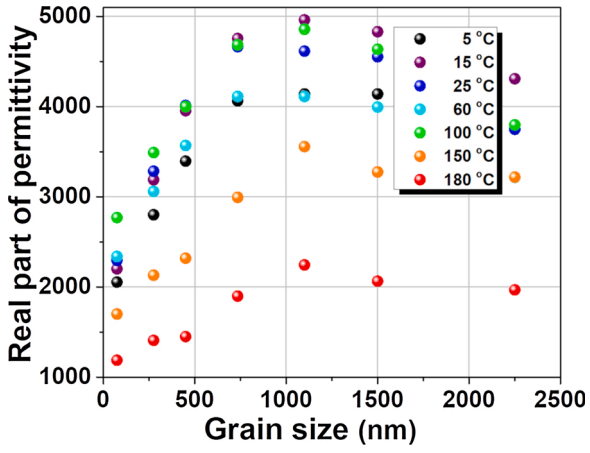

Fig. 16. Grain size dependence of low-field permittivity determined at various temperatures (f = 10 kHz).

In conclusion, the universal behaviour of permittivity maximum around GS ~ 1100 nm was found by low-field impedance spectroscopy analyses, it was further confirmed by the zero field permittivity determined by Rayleigh analysis, but, most interestingly, it was also detected in states where the domain wall contributions should be minimized, *e.g.* under high dc field close to the saturation and above the Curie temperature, where ferroelectric domains should disappear. One should note that, by considering the density variations in the present set of ceramics in the range of 94–98 %, the enhanced permittivity around the critical size, determined from different experiments and under various conditions, does not scale with the density variation. In a recent paper [91], a numerical route based on finite-element method was developed to compute the effective permittivity of full-density ceramics by considering the experimentally determined permittivity of ceramics with a certain degree of variable porosity. Based on this method, the deviation of the effective permittivity from the value corresponding to the full dense ceramic is of ~3 % and ~10 %, for a relative density of 98 % and 94 %, respectively. Even by considering such permittivity variations, the maximum at the critical grain size is maintained for the values corresponding to the full dense ceramics (as shown in Fig. S9, Supplementary Material), as for the experimentally determined ones.

With the present data, we cannot explain if the phase coexistence in the present series of samples plays some role on the critical behaviour around 1 μm and it shows that there are still some features to be further investigated in $BaTiO_3$ with intermediate range of GS.

5. Electron microscopy study of defects in $BaTiO_3$ at room temperature

As mentioned in Sec. III A, the room temperature phase coexistence (*e.g.* O/T or other polymorphs) or predominant O state instead of the usual T was sometimes reported in $BaTiO_3$ ceramics, but rarely discussed, with the exception of some cases, when it was assigned to specific processing parameters [7,32] or to domain texturing produced by mechanical stress induced by ceramic surface polishing or cutting, due to the ferroelastic nature of 90 ° domains [37,39]. In the present set of ceramics, the phase coexistence around room temperature was not observed in a specific range of GSs and is not related to surface mechanical treatment of ceramics, being rather a volume effect.

To search for specific nanoscale features that could explain the phase coexistence, a detailed nanoscale analysis was performed by electron microscopy – in transmission (TEM) and scanning transmission (STEM) modes on the starting powders and on the ceramic sintered at 1150 °C for 1 h. Fig. 17(a) shows the TEM image of $BaTiO_3$ powder, indicating

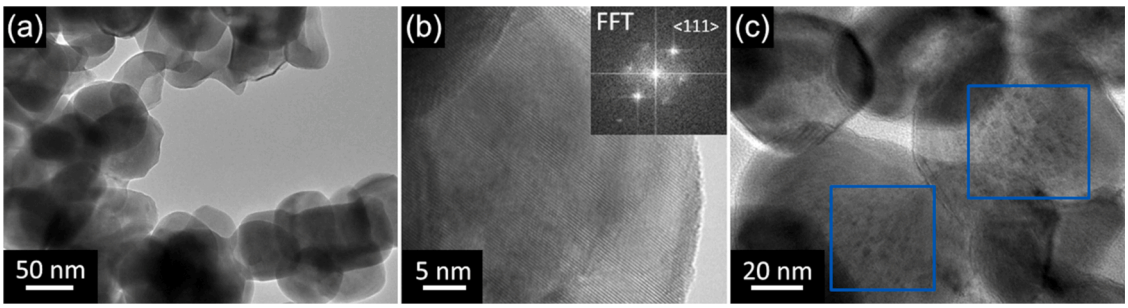

Fig. 17. TEM image of $BaTiO_3$ powder showing grains a few tens of nm in size (a), well crystalline grain in <111> zone axis with corresponding Fast Fourier Transform (FFT) (b) and grains with defects marked with blue rectangles (c).

well-defined faceted grains, with uniform shape and average particle size of about 50−60 nm, as also observed by the SEM analysis (Fig. 4). Grains are crystalline [Fig. 17(b)], confirming a high degree of crystallinity of the starting powders. Grains are chemically homogeneous, without core-shell structure, as shown by energy dispersive X-ray spectroscopy (EDXS) mapping and by electron-energy loss spectroscopy (EELS) analysis performed in the centre of the grains and at their edges in Fig. S10, *Supplementary material*. As shown in Fig. 17(c), defects (marked with blue rectangles) were observed in some grains. It was reported in literature that hydrothermally synthesized $BaTiO_3$ powders usually may contain defects, due to the use of high pressure processing [92]. In such $BaTiO_3$ powders, a large population of proton defects attached nearby O^{2-} ions, thus generating ($OH^{\bullet}$) defects were usually found [93,94]. According to Hennings *et al.* [92,95], the electroneutrality is realized by the formation of both Barium and Titanium vacancies which generate in the final powder product a large number of small nanosized intragranular pores and/or structural defects. By increasing temperature such vacancies migrate and they may be partially or completely eliminated or transformed into particle internal porosity or structural defects in the crystalline lattice [94,96,97]. The structural defects are usually accompanied by structural/microstructural localized internal stresses, which in turn may affect the final properties of films or ceramics consolidated from hydrothermal powders [98].

The powder particles used in this study do not contain any internal porosity, as found by other authors [92], but regions with extended planar defects were observed in several places, as for example the ones marked in Fig. 17(c). In addition, defects in various grains, oriented in different zone axis, were further analysed by STEM at nanoscale level. Low angle annular dark field (LAADF) images in Fig. 18 show strained, up to 5 nm long planar defects forming a loop at {100} planes. The contrast in the LAADF images indicates lattice distortion in the defect region and with that, associated local strain. No cation vacancy formation was observed at the defects. The EELS analysis revealed that oxidation state of Ti is 4^+, both on the location of defects and in the grain matrix and no modification of composition assigned to the defect exists. The presence of high strained regions inside the hydrothermally prepared $BaTiO_3$ nanoparticles was also reported in Ref. [99] by variations of electron diffraction contrast across these particles in the TEM images and were also assigned to the presence of lattice defects like OH^- ions and their compensation by cation vacancies.

The presence of defects in the starting hydrothermally synthesised powder is usually at the origin of structural defects in the volume of consolidated ceramics, which strongly impact their functional properties. The examination of $BaTiO_3$ ceramic sintered at 1150 °C indicates the presence in some ceramic grains of a large number of extended strained defects (possibly dislocations), mostly located inside the grain cores [Fig. 19(a)] with irregular shape and distribution. The grain boundaries seem rather free of such defects, indicating that most probably the grain boundaries allowed the equilibration of the inhomogeneous field stress existing in the starting powders during the grain growth stage, when sintering the ceramics. At atomic level, HAADF-STEM images show well-defined ceramic grain boundaries separating single-crystalline regions, as shown in Fig. 19(b), with terrace-like aspect, free of defects, secondary phases or impurities. The formation of dislocation loops was reported in $BaTiO_3$ ceramics for multilayer ceramic capacitors [100] and in pure and Ca-doped $BaTiO_3$ ceramics sintered in reduced atmosphere [101], where such defects were considered to be related to the oxygen vacancies existing in the perovskite lattice, due to the processing under low oxygen partial pressure. However, no data concerning the possible existence of extended structural defects in the starting powders, or on its synthesis method and purity were provided. The present set of ceramics have been firstly subjected to a fast SPS consolidation step under reducing atmosphere, in which most probably the initial existing stresses assigned to the observed dislocations could not be released under the high

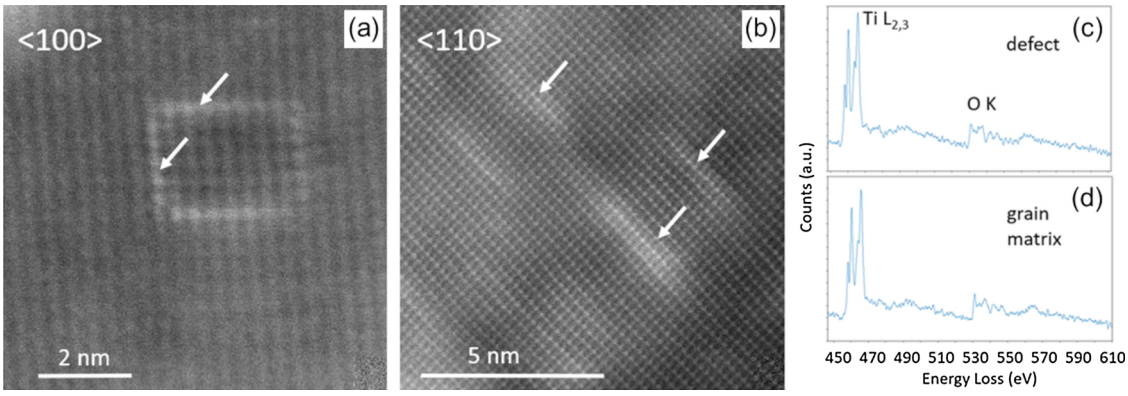

Fig. 18. LAADF-STEM images of planar defects on {100} planes (marked with arrows) in <100> (a) and <110> (b) zone axis, with experimental EEL spectra acquired on defect (c) and on grain matrix (d) with indicated Ti $L_{2,3}$ and O K edges.

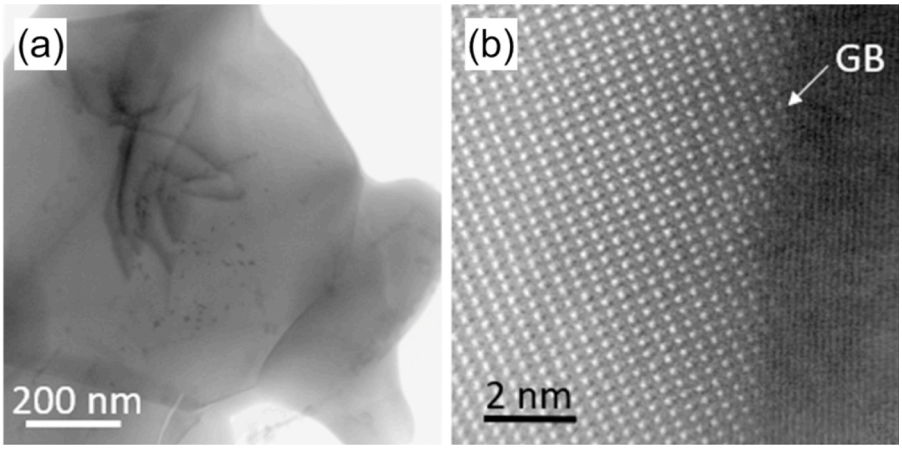

Fig. 19. $BaTiO_3$ ceramic sintered at 1150 °C: BF- STEM image of dislocations within the grain (a), HAADF-STEM image (b) of a clean grain boundary (GB).

non-equilibrium conditions and in addition, oxygen vacancies were generated by the reducing conditions specific to SPS consolidation. During the pressureless sintering second step allowing grain growth, followed by slow cooling, the large majority of oxygen vacancies were eliminated and stress was partially accommodated and released, mostly on grain boundaries. However, the majority of dislocations existing in the starting powders lead to a large number of strained defects inside the ceramic grains, whose density is expected to be higher as GS is smaller.

Even if there is not a full agreement concerning the direct role of the structural defects on the functional properties of ferroelectric ceramics, it is generally accepted that besides the charged defects, structural point defects, dislocations, line defects or volume defects in the crystal lattices and their interactions govern the properties of many ferro/piezoelectric materials [102]. In addition, the elastic distortions of regular lattices around dislocations can give rise to a strain field with which the atomic impurities or point defects might interact, thus influencing many areas of materials' properties [103]. Nanoscale studies realized on ferroelectric films indicated that dislocations play a role both in the stabilization of specific equilibrium domain structures (*i.e.* in defining the domain pattern), as well as on their mobility and reversible/irreversible interaction with electric and stress fields [104]. Dislocations have been observed to serve as nucleating sites for 90 ° domains in barium titanate or in other ferroelectric perovskites and prevent motion of the 90 ° boundaries by pinning them through a strain interaction and inducing unstable polarization in ferroelectric films, thus deteriorating the ferroelectric switching performances [105]. Similarly, the dislocations were proved to enhance some otherwise unfavourable change in the direction of polarization within the ferroelectric [106] or to facilitate the formation of 90 ° domain walls, which further contributes extrinsically to the dielectric and piezoelectric properties [107]. By determining the local stress field and changing the local domain structure and domain wall mobility, all the dielectric, ferroelectric, piezo- and pyroelectric properties, but also the ferroelectric stability, phase composition and temperature ranges for the phase coexistence may be affected by dislocations [108,109]. As recently demonstrated [110], dislocations present a multiscale interaction with the fundamental order and field parameters in bulk ferroelectric oxides (polarization and strain) and if properly used, it may allow the tuning of the dielectric and electromechanical properties. Therefore, the presence of a large number of strained nanoscale dislocations in the ceramic volume may play a role in determining unusual observed properties, *i.e.* the existence of a large temperature range around room temperature with coexistence of polymorphs instead of pure T phase, the stabilization of polar nanodomains with contributions on permittivity up to high temperatures and under high dc fields close to the saturation, and the overall large values of permittivity and polarization with respect to ones previously reported for $BaTiO_3$ ceramics with similar GSs [3,4].

6. Conclusions

The equilibrium T state is typical to $BaTiO_3$ ceramics around room temperature, but there are many reports indicating the presence of O, low symmetry phases or mixture of polymorphs with variable weights and stability ranges, mostly as result of specific processing ways or by surface domain texturing. Calculations based on Landau-based models indicate the possible existence of phase superposition around room temperature, irrespective of grain sizes, when examining the metastable free energy states. In such systems, field-induced modifications of phase composition take place, with a further influence on their functional properties (in particular, ones determined in poled ceramics, as piezo- and pyroelectric properties). The present study investigated $BaTiO_3$ ceramics with phase superposition around room temperature in order to observe if phase coexistence impacts on their grain-size dependent functional (structural, dielectric, calorimetric, Raman, ferroelectric and tunability) properties. For all the investigated grain sizes, from 75 nm to 2.25 μm, multiple peaks appear near the 002_{PC} region and exist within a large temperature rate, indicating a phase superposition. Preliminary structural calculations indicated at room temperature a mixture of O and T states for all the GSs, but the possible existence of other phases is not excluded. At nanoscale, these ceramics are characterized by the presence of strained extended defects (*e.g.* dislocations) originated from defects existing in the starting powders and such defects may play a role in the stabilization of O state and multiphase character around room temperature. Typical reduction of Curie temperature and increasing of O-T transition temperature when reducing grain size was confirmed by structural, Raman, calorimetry and dielectric investigations. As reported by many authors, a maximum of low-field permittivity around 1 μm grain size is detected in the present series of ceramics. The largely accepted interpretation concerning this maximum considers the extrinsic contribution of domain walls on the permittivity, which find a maximum of their density and mobility around this critical grain size. However, the present study revealed the existence of such a permittivity maximum around 1 μm grain size in states where the role of domain walls is minimal, or even absent: (i) in the paraelectric state, at ~180 °C (where ferroelectric domains should disappear), and (ii) under high dc field $E_{dc} = 25$ kV/cm, where a monodomain state should be established (or at least the number of domain walls is strongly reduced). In spite of a large number of papers concerning size effects in $BaTiO_3$ ceramics, no one reported permittivity values in the paraelectric state or at saturation as a function of grain size and therefore, we cannot conclude if the present results are universal or they are related to these specific ceramics with phase coexistence and with nanoscale extended strained defects. If the role of domain walls is eliminated or strongly diminished, either intrinsic contribution to this maximum should be again reconsidered, or contributions from mobile nanopolar regions as well as of other

interphase boundaries or defects, showing enhanced mobility around the critical GS ~ 1 μm, may contribute to preserve a dielectric maximum in $BaTiO_3$ ceramics in the absence of large-scale ferroelectric domains.

Summary of novel conclusions

The paper presents the functional properties of $BaTiO_3$ ceramics at intermediate grain size range (75 nm to 2.25 μm) with polymorph coexistence around room temperature. The novelty with respect to previous multiple publications in this topic is given by the fact that the present set of ceramics is not purely tetragonal at room temperature as usually $BaTiO_3$ is, the possible role of phase superposition on the grain size dependent properties not being previously analysed or reported. The permittivity values are among the highest reported, possibly as result of the phase superposition. The most interesting feature, not reported elsewhere, is the persistence of permittivity maximum (at around 1 μm) even above Curie temperature and under high dc field at saturation, where the domain walls contribution is minimal, raising questions about the largely accepted interpretation concerning the role of domain walls (density and dynamics) on the permittivity maximum. We also offer an indirect explanation on the fact that d_{33} maximum is not so well defined in literature as the permittivity maximum around 1 μm, by showing that in multiphase systems, field-induced modifications of polymorph compositions are likely and this feature impacts on the reported values of d_{33}, since the piezoelectric measurements involve sample poling under high dc fields.

Data availability

Data will be made available on request.

Declaration of Competing Interest

The authors declare that they have no known competing financial interests or personal relationships that could have appeared to influence the work reported in this paper.

Acknowledgements

This study was financially supported by the Romanian UEFISCDI PN-III-P4-ID-PCE-2016-0817 (FerroScale) grant. Calorimetry and microstructural studies were performed within PN-III-P4-ID-PCCF-2016-0175 grant (HighKDevice). A. Bencan acknowledges funding from the Slovenian Research Agency within P2-0105 program and J2-2497 project. Brigita Kmet is acknowledged for STEM sample preparation. M. Avakian and J. Jones acknowledge support from the U.S. National Science Foundation under award number DMR-1409399 for summer undergraduate studies in 2019. The high temperature XRD experiments were performed at the Analytical Instrumentation Facility (AIF) at North Carolina State University, which is supported by the State of North Carolina and the National Science Foundation (award number ECCS-2025064). The AIF is a member of the North Carolina Research Triangle Nanotechnology Network (RTNN), a site in the U.S. National Nanotechnology Coordinated Infrastructure (NNCI). J. Jones acknowledges additional support from the U.S. National Science Foundation under award number DMR-2004455 to facilitate interpretation and dissemination of results. M. Deluca has received funding from the European Research Council (ERC) under the European Union's Horizon 2020 research and innovation program (grant agreement no. 817190).

Appendix A. Supplementary data

Supplementary material related to this article can be found, in the online version, at doi:https://doi.org/10.1016/j.jeurceramsoc.2021.12.024.

References

[1] J. Ho, T.R. Jow, S. Boggs, Historical introduction to capacitor technology, IEEE Electr. Insul. Mag. 26 (2010) 20–25, https://doi.org/10.1109/MEI.2010.5383924.
[2] J.F. Ihlefeld, D.T. Harris, R. Keech, J.L. Jones, J.-P. Maria, S. Trolier-McKinstry, Scaling effects in perovskite ferroelectrics: fundamental limits and process-structure-property relations, J. Am. Ceram. Soc. 99 (2016) 2537–2557, https://doi.org/10.1111/jace.14387.
[3] L. Mitoseriu, L.P. Curecheriu, Nanostructured barium titanate ceramics: intrinsic versus extrinsic size effects, in: M. Algueró, J.M. Gregg, L. Mitoseriu (Eds.), Nanoscale Ferroelectr. Multiferroics, John Wiley & Sons, Ltd, Chichester, UK, 2016, pp. 473–511, https://doi.org/10.1002/9781118935743.ch15.
[4] V. Buscaglia, C.A. Randall, Size and scaling effects in barium titanate. An overview, J. Eur. Ceram. Soc. 40 (2020) 3744–3758, https://doi.org/10.1016/j.jeurceramsoc.2020.01.021.
[5] A.V. Polotai, A.V. Ragulya, C.A. Randall, Preparation and size effect in pure nanocrystalline barium titanate ceramics, Ferroelectrics 288 (2003) 93–102, https://doi.org/10.1080/00150190390211972.
[6] Z. Zhao, V. Buscaglia, M. Viviani, M.T. Buscaglia, L. Mitoseriu, A. Testino, M. Nygren, M. Johnsson, P. Nanni, Grain-size effects on the ferroelectric behavior of dense nanocrystalline $BaTiO_3$ ceramics, Phys. Rev. B 70 (2004), 024107, https://doi.org/10.1103/PhysRevB.70.024107.
[7] X. Deng, X. Wang, H. Wen, A. Kang, Z. Gui, L. Li, Phase transitions in nanocrystalline barium titanate ceramics prepared by spark plasma sintering, J. Am. Ceram. Soc. 89 (2006) 1059–1064, https://doi.org/10.1111/j.1551-2916.2005.00836.x.
[8] L. Curecheriu, M.T. Buscaglia, V. Buscaglia, Z. Zhao, L. Mitoseriu, Grain size effect on the nonlinear dielectric properties of barium titanate ceramics, Appl. Phys. Lett. 97 (2010) 95–98, https://doi.org/10.1063/1.3526375.
[9] L.G.D. Silveira, M.F.S. Alves, L.F. Cótica, R.A.M. Gotardo, W.J. Nascimento, D. Garcia, J.A. Eiras, I.A. Santos, Dielectric investigations in nanostructured tetragonal $BaTiO_3$ ceramics, Mater. Res. Bull. 48 (2013) 1772–1777, https://doi.org/10.1016/j.materresbull.2013.01.009.
[10] Y. Huan, X. Wang, J. Fang, L. Li, Grain size effects on piezoelectric properties and domain structure of $BaTiO_3$ ceramics prepared by two-step sintering, J. Am. Ceram. Soc. 96 (2013) 3369–3371, https://doi.org/10.1111/jace.12601.
[11] Y. Huan, X. Wang, J. Fang, L. Li, Grain size effect on piezoelectric and ferroelectric properties of $BaTiO_3$ ceramics, J. Eur. Ceram. Soc. 34 (2014) 1445–1448, https://doi.org/10.1016/J.JEURCERAMSOC.2013.11.030.
[12] D. Ghosh, A. Sakata, J. Carter, P.A. Thomas, H. Han, J.C. Nino, J.L. Jones, Domain wall displacement is the origin of superior permittivity and piezoelectricity in $BaTiO_3$ at intermediate grain sizes, Adv. Funct. Mater. 24 (2014) 885–896, https://doi.org/10.1002/adfm.201301913.
[13] Y. Tan, J. Zhang, Y. Wu, C. Wang, V. Koval, B. Shi, H. Ye, R. McKinnon, G. Viola, H. Yan, Unfolding grain size effects in barium titanate ferroelectric ceramics, Sci. Rep. 5 (2015) 15–21, https://doi.org/10.1038/srep09953.
[14] B. Dai, P. Zheng, W. Bai, F. Wen, L. Li, W. Wu, Z. Ying, L. Zheng, Direct and converse piezoelectric grain-size effects in $BaTiO_3$ ceramics with different Ba/Ti ratios, J. Eur. Ceram. Soc. 38 (2018) 4212–4219, https://doi.org/10.1016/j.jeurceramsoc.2018.05.011.
[15] T. Hoshina, S. Hatta, H. Takeda, T. Tsurumi, Grain size effect on piezoelectric properties of $BaTiO_3$ ceramics, Jpn. J. Appl. Phys. 57 (2018), 0902BB, https://doi.org/10.7567/JJAP.57.0902BB.
[16] W.R. Buessem, L.E. Cross, A.K. Goswami, Phenomenological theory of high permittivity in fine-grained barium titanate, J. Am. Ceram. Soc. 49 (1966) 33–36, https://doi.org/10.1111/J.1151-2916.1966.TB13144.X.
[17] K. Kinoshita, A. Yamaji, Grain-size effects on dielectric properties in barium titanate ceramics, J. Appl. Phys. 47 (1976) 371–373, https://doi.org/10.1063/1.322330.
[18] A.J. Bell, A.J. Moulson, L.E. Cross, The effect of grain size on the permittivity of $BaTiO_3$, Ferroelectrics 54 (1984) 147–150, https://doi.org/10.1080/00150198408215837.
[19] G. Arlt, Twinning in ferroelectric and ferroelastic ceramics: stress relief, J. Mater. Sci. 25 (1990) 2655–2666, https://doi.org/10.1007/BF00584864.
[20] G. Arlt, D. Hennings, G. De With, Dielectric properties of fine-grained barium titanate ceramics, J. Appl. Phys. 58 (1985) 1619–1625, https://doi.org/10.1063/1.336051.
[21] G. Arlt, N.A. Pertsev, Force constant and effective mass of 90°domain walls in ferroelectric ceramics, J. Appl. Phys. 70 (1991) 2283–2289, https://doi.org/10.1063/1.349421.
[22] N.A. Pertsev, G. Arlt, Forced translational vibrations of 90° domain walls and the dielectric dispersion in ferroelectric ceramics, J. Appl. Phys. 74 (1998) 4105, https://doi.org/10.1063/1.354457.
[23] A.J. Bell, Grain size effects in barium titanate-revisited, in: Proc. 1994 IEEE Int. Symp. Appl. Ferroelectr., IEEE, 1994, pp. 14–17, https://doi.org/10.1109/ISAF.1994.522286.
[24] P. Zheng, J.L. Zhang, Y.Q. Tan, C.L. Wang, Grain-size effects on dielectric and piezoelectric properties of poled $BaTiO_3$ ceramics, Acta Mater. 60 (2012) 5022–5030, https://doi.org/10.1016/j.actamat.2012.06.015.
[25] L. Curecheriu, S.-B.B. Balmus, M.T. Buscaglia, V. Buscaglia, A. Ianculescu, L. Mitoseriu, Grain size-dependent properties of dense nanocrystalline barium titanate ceramics, J. Am. Ceram. Soc. 95 (2012) 3912–3921, https://doi.org/10.1111/j.1551-2916.2012.05409.x.

[26] C. Fang, L. Chen, D. Zhou, Influence of domain on grain size effects of the dielectric properties of $BaTiO_3$ nanoceramics and nanoparticles, Phys. B Condens. Matter. 409 (2013) 83–86, https://doi.org/10.1016/J.PHYSB.2012.10.016.

[27] K. Tsuji, A. Ndayishimiye, S. Lowum, R. Floyd, K. Wang, M. Wetherington, J. P. Maria, C.A. Randall, Single step densification of high permittivity $BaTiO_3$ ceramics at 300 °C, J. Eur. Ceram. Soc. 40 (2020) 1280–1284, https://doi.org/10.1016/j.jeurceramsoc.2019.12.022.

[28] S. Lin, T. Lü, C. Jin, X. Wang, Size effect on the dielectric properties of $BaTiO_3$ nanoceramics in a modified Ginsburg-Landau-Devonshire thermodynamic theory, Phys. Rev. B - Condens. Matter Mater. Phys. 74 (2006), 134115, https://doi.org/10.1103/PhysRevB.74.134115.

[29] Y.L. Li, L.E. Cross, L.Q. Chen, A phenomenological thermodynamic potential for $BaTiO_3$ single crystals, J. Appl. Phys. 98 (2005), 064101, https://doi.org/10.1063/1.2042528.

[30] N. Horchidan, L. Padurariu, C.E. Ciomaga, L. Curecheriu, M. Airimioaei, F. Doroftei, F. Tufescu, L. Mitoseriu, Room temperature phase superposition as origin of enhanced functional properties in $BaTiO_3$ - based ceramics, J. Eur. Ceram. Soc. 40 (2020) 1258–1268, https://doi.org/10.1016/j.jeurceramsoc.2019.11.088.

[31] J. Petzelt, Dielectric grain-size effect in high-permittivity ceramics, Ferroelectrics 400 (2010) 117–134, https://doi.org/10.1080/00150193.2010.505511.

[32] N. Ma, B.P. Zhang, W.G. Yang, D. Guo, Phase structure and nano-domain in high performance of $BaTiO_3$ piezoelectric ceramics, J. Eur. Ceram. Soc. 32 (2012) 1059–1066, https://doi.org/10.1016/j.jeurceramsoc.2011.11.014.

[33] A.K. Kalyani, K. Brajesh, A. Senyshyn, R. Ranjan, Orthorhombic-tetragonal phase coexistence and enhanced piezo-response at room temperature in Zr, Sn, and Hf modified $BaTiO_3$, Appl. Phys. Lett. 104 (2014), 252906, https://doi.org/10.1063/1.4885516.

[34] J. Gao, Y. Wang, Y. Liu, X. Hu, X. Ke, L. Zhong, Y. He, X. Ren, Enhancing dielectric permittivity for energy-storage devices through tricritical phenomenon, Sci. Rep. 7 (2017) 1–10, https://doi.org/10.1038/srep40916.

[35] A.C. Larson, R.B. Von Dreele, GSAS - General Structure Analysis System, Los Alamos National Laboratory, Los Alamos, USA, 2001.

[36] F.-M. Tufescu, U. Alexandru, I. Cuza, A. Ianculescu, F.M. Tufescu, L. Curecheriu, A. Ianculescu, C.E. Ciomaga, L. Mitoseriu, High-voltage tunability measurements of the $BaZr_xTi_{1-x}O_3$ ferroelectric ceramics, J. Optoelectron. Adv. Mater. 10 (2008) 1894–1897 (Accessed July 22, 2020), https://www.researchgate.net/publication/232716156.

[37] M. Hammer, C. Monty, A. Endriss, M.J. Hoffmann, Correlation between surface texture and chemical composition in undoped, hard, and soft piezoelectric PZT ceramics, J. Am. Ceram. Soc. 81 (1998) 721–724, https://doi.org/10.1111/j.1151-2916.1998.tb02397.x.

[38] J.L. Jones, E.B. Slamovich, K.J. Bowman, Domain texture distributions in tetragonal lead zirconate titanate by x-ray and neutron diffraction, J. Appl. Phys. 97 (2005), 034113, https://doi.org/10.1063/1.1849821.

[39] G.P. Khanal, S. Kim, I. Fujii, S. Ueno, C. Moriyoshi, Y. Kuroiwa, S. Wada, Effect of thermal annealing on crystal structures and electrical properties in $BaTiO_3$ ceramics, J. Appl. Phys. 124 (2018), 034102, https://doi.org/10.1063/1.5023814.

[40] E.C. Subbarao, M.C. McQuarrie, W.R. Buessem, Domain effects in polycrystalline barium titanate, J. Appl. Phys. 28 (1957) 1194–1200, https://doi.org/10.1063/1.1722606.

[41] B.W. Lee, K.H. Auh, Effect of grain size and mechanical processing on the dielectric properties of $BaTiO_3$, J. Mater. Res. 10 (1995) 1418–1423, https://doi.org/10.1557/JMR.1995.1418.

[42] X. Li, W.Y. Shih, J.S. Vartuli, D.L. Milius, I.A. Aksay, W.H. Shih, Effect of a transverse tensile stress on the electric-field-induced domain reorientation in soft PZT: in situ XRD study, J. Am. Ceram. Soc. 85 (2002) 844–850, https://doi.org/10.1111/j.1151-2916.2002.tb00182.x.

[43] C.J. Xiao, C.Q. Jin, X.H. Wang, Crystal structure of dense nanocrystalline $BaTiO_3$ ceramics, Mater. Chem. Phys. 111 (2008) 209–212, https://doi.org/10.1016/j.matchemphys.2008.01.020.

[44] V. Buscaglia, M.T. Buscaglia, M. Viviani, L. Mitoseriu, P. Nanni, V. Trefiletti, P. Piaggio, I. Gregora, T. Ostapchuk, J. Pokorný, J. Petzelt, Grain size and grain boundary-related effects on the properties of nanocrystalline barium titanate ceramics, J. Eur. Ceram. Soc. 26 (2006) 2889–2898, https://doi.org/10.1016/j.jeurceramsoc.2006.02.005.

[45] G. Picht, H. Kungl, M. BÄurer, M.J. Hoffmann, High electric field induced strain in solid-state route processed barium titanate ceramics, Funct. Mater. Lett. 3 (2010) 59–64, https://doi.org/10.1142/S1793604710000889.

[46] D.S. Keeble, P.A. Thomas, On the tetragonality of the room-temperature ferroelectric phase of barium titanate, $BaTiO_3$, J. Appl. Crystallogr. 42 (2009) 480–484, https://doi.org/10.1107/S0021889809008310.

[47] T.T.A. Lummen, Y. Gu, J. Wang, S. Lei, F. Xue, A. Kumar, A.T. Barnes, E. Barnes, S. Denev, A. Belianinov, M. Holt, A.N. Morozovska, S.V. Kalinin, L.-Q. Chen, V. Gopalan, Thermotropic phase boundaries in classic ferroelectrics, Nat. Commun. 5 (2014) 3172, https://doi.org/10.1038/ncomms4172.

[48] A.K. Kalyani, D.K. Khatua, B. Loukya, R. Datta, A.N. Fitch, A. Senyshyn, R. Ranjan, Metastable monoclinic and orthorhombic phases and electric field induced irreversible phase transformation at room temperature in the lead-free classical ferroelectric $BaTiO_3$, Phys. Rev. B - Condens. Matter Mater. Phys. 91 (2015), 104104, https://doi.org/10.1103/PhysRevB.91.104104.

[49] Y.T. Shao, J.M. Zuo, Nanoscale symmetry fluctuations in ferroelectric barium titanate, $BaTiO_3$, Acta Crystallogr. Sect. B Struct. Sci. Cryst. Eng. Mater. 73 (2017) 708–714, https://doi.org/10.1107/S2052520617008496.

[50] G. Canu, G. Confalonieri, M. Deluca, L. Curecheriu, M.T. Buscaglia, M. Asandulesa, N. Horchidan, M. Dapiaggi, L. Mitoseriu, V. Buscaglia, Structure-property correlations and origin of relaxor behaviour in $BaCe_xTi_{1-x}O_3$, Acta Mater. 152 (2018) 258–268, https://doi.org/10.1016/j.actamat.2018.04.038.

[51] Upendra A. Joshi, Songhak Yoon, Sunggi Baik, Jae Sung Lee, Surfactant-free hydrothermal synthesis of highly tetragonal barium titanate nanowires: a structural investigation, J. Phys. Chem. B 110 (2006) 12249–12256, https://doi.org/10.1021/JP0600110.

[52] A. Gajović, J.V. Pleština, K. Žagar, M. Plodinec, S. Šturm, M. Čeh, Temperature-dependent Raman spectroscopy of $BaTiO_3$ nanorods synthesized by using a template-assisted sol-gel procedure, J. Raman Spectrosc. 44 (2013) 412–420, https://doi.org/10.1002/jrs.4206.

[53] J.D. Freire, R.S. Katiyar, Lattice dynamics of crystals with tetragonal $BaTiO_3$ structure, Phys. Rev. B 37 (1988) 2074–2085, https://doi.org/10.1103/PhysRevB.37.2074.

[54] G. Philippot, M. Albino, R. Epherre, G. Chevallier, Y. Beynet, C. Manière, A. Weibel, A. Peigney, M. Deluca, C. Elissalde, M. Maglione, C. Aymonier, C. Estournès, Ferroelectric ceramics: local distortions in nanostructured ferroelectric ceramics through strain tuning (Adv. Electron. Mater. 10/2015), Adv. Electron. Mater. 1 (2015), https://doi.org/10.1002/aelm.201570036.

[55] O. Bidault, P. Goux, M. Kchikech, M. Belkaoumi, M. Maglione, Space-charge relaxation in perovskites, Phys. Rev. B 49 (1994) 7868–7873, https://doi.org/10.1103/PhysRevB.49.7868.

[56] M. Frey, D. Payne, Grain-size effect on structure and phase transformations for barium titanate, Phys. Rev. B - Condens. Matter Mater. Phys. 54 (1996) 3158–3168, https://doi.org/10.1103/PhysRevB.54.3158.

[57] M.H. Frey, Z. Xu, P. Han, D.A. Payne, Role of interfaces on an apparent grain size effect on the dielectric properties for ferroelectric barium titanate ceramics, Ferroelectrics 206–207 (1998) 337–353, https://doi.org/10.1080/00150199808009168.

[58] A.Y. Emelyanov, N.A. Pertsev, S. Hoffmann-Eifert, U. Böttger, R. Waser, Grain-boundary effect on the Curie-Weiss law of ferroelectric ceramics and polycrystalline thin films: calculation by the method of effective medium, J. Electroceram. 9 (2002) 5–16, https://doi.org/10.1023/A:1021665300233.

[59] J. Petzelt, I. Rychetský, Effective dielectric function in high-permittivity ceramics and films, Ferroelectrics 316 (2005) 89–95, https://doi.org/10.1080/00150190590963183.

[60] T. Ostapchuk, J. Petzelt, M. Savinov, V. Buscaglia, L. Mitoseriu, Grain-size effect in $BaTiO_3$ ceramics: study by far infrared spectroscopy, Phase Transitions 79 (2006) 361–373, https://doi.org/10.1080/01411590600892047.

[61] H.T. Martirena, J.C. Burfoot, Grain-size effects on properties of some ferroelectric ceramics, J. Phys. C Solid State Phys. 7 (1974) 3182–3192, https://doi.org/10.1088/0022-3719/7/17/024.

[62] T. Hoshina, Y. Kigoshi, S. Hatta, H. Takeda, T. Tsurumi, Domain contribution to dielectric properties of fine-grained $BaTiO_3$ ceramics, Jpn. J. Appl. Phys. 48 (2009), 09KC01, https://doi.org/10.1143/JJAP.48.09KC01.

[63] L. Padurariu, L. Curecheriu, V. Buscaglia, L. Mitoseriu, Field-dependent permittivity in nanostructured $BaTiO_3$ ceramics: modeling and experimental verification, Phys. Rev. B - Condens. Matter Mater. Phys. 85 (2012) 1–9, https://doi.org/10.1103/PhysRevB.85.224111.

[64] J.L. Zhu, S. Lin, S.M. Feng, L.J. Wang, Q.Q. Liu, C.Q. Jin, X.H. Wang, C.F. Zhong, L.T. Li, W. Cao, Pressure tuned ferroelectric reentrance in nano-$BaTiO_3$ ceramics, J. Appl. Phys. 112 (2012), 124107, https://doi.org/10.1063/1.4770358.

[65] S. Ma, X. Wang, J. Zhou, L. Li, C.Q. Sun, Thermal stability of the nanostructured $BaTiO_3$ determined by long and short range interactions: a dual-shell model, J. Appl. Phys. 107 (2010), 064102, https://doi.org/10.1063/1.3331958.

[66] M.T. Buscaglia, M. Viviani, V. Buscaglia, L. Mitoseriu, A. Testino, P. Nanni, Z. Zhao, M. Nygren, C. Harnagea, D. Piazza, C. Galassi, High dielectric constant and frozen macroscopic polarization in dense nanocrystalline $BaTiO_3$ ceramics, Phys. Rev. B - Condens. Matter Mater. Phys. 73 (2006), 064114, https://doi.org/10.1103/PhysRevB.73.064114.

[67] Y. Chen, H. Ye, X. Wang, Y. Li, X. Yao, Grain size effects on the electric and mechanical properties of submicron $BaTiO_3$ ceramics, J. Eur. Ceram. Soc. 40 (2020) 391–400, https://doi.org/10.1016/j.jeurceramsoc.2019.09.033.

[68] T. Takeuchi, C. Capiglia, N. Balakrishnan, Y. Takeda, H. Kageyama, Preparation of fine-grained $BaTiO_3$ ceramics by spark plasma sintering, J. Mater. Res. 17 (2002) 575–581, https://doi.org/10.1557/JMR.2002.0081.

[69] G. Arlt, The influence of microstructure on the properties of ferroelectric ceramics, Ferroelectrics 104 (1990) 217–227, https://doi.org/10.1080/00150199008223825.

[70] A.S. Shaikh, R.W. Vest, G.M. Vest, Dielectric properties of ultrafine grained BaTiO/sub 3/, IEEE Trans. Ultrason. Ferroelectr. Freq. Control. 36 (1989) 407–412, https://doi.org/10.1109/58.31776.

[71] T. Hoshina, T. Furuta, Y. Kigoshi, S. Hatta, N. Horiuchi, H. Takeda, T. Tsurumi, Size effect of nanograined $BaTiO_3$ ceramics fabricated by aerosol deposition method, J. Appl. Phys. 49 (2010), 09MC02, https://doi.org/10.1143/JJAP.49.09MC02.

[72] T. Hoshina, Size effect of barium titanate: fine particles and ceramics, J. Ceram. Soc. Jpn. 121 (2013) 156–161, https://doi.org/10.2109/jcersj2.121.156.

[73] H. Gong, X. Wang, S. Zhang, H. Wen, L. Li, Grain size effect on electrical and reliability characteristics of modified fine-grained $BaTiO_3$ ceramics for MLCCs, J. Eur. Ceram. Soc. 34 (2014) 1733–1739, https://doi.org/10.1016/j.jeurceramsoc.2013.12.028.

[74] Q.M. Zhang, W.Y. Pan, S.J. Jang, L.E. Cross, Domain wall excitations and their contributions to the weak-signal response of doped lead zirconate titanate ceramics, J. Appl. Phys. 64 (1998) 6445, https://doi.org/10.1063/1.342059.

[75] D. Damjanovic, M. Demartin, The Rayleigh law in piezoelectric ceramics, J. Phys. D. Appl. Phys. 29 (1996) 2057–2060, https://doi.org/10.1088/0022-3727/29/7/046.

[76] R.E. Eitel, T.R. Shrout, C.A. Randall, Nonlinear contributions to the dielectric permittivity and converse piezoelectric coefficient in piezoelectric ceramics, J. Appl. Phys. 99 (2006), 124110, https://doi.org/10.1063/1.2207738.

[77] J.E. García, R. Prez, D.A. Ochoa, A. Albareda, M.H. Lente, J.A. Eiras, Evaluation of domain wall motion in lead zirconate titanate ceramics by nonlinear response measurements, J. Appl. Phys. 103 (2008), 054108, https://doi.org/10.1063/1.2894595.

[78] C. Borderon, R. Renoud, M. Ragheb, H.W. Gundel, Description of the low field nonlinear dielectric properties of ferroelectric and multiferroic materials, Appl. Phys. Lett. 98 (2011), 112903, https://doi.org/10.1063/1.3567777.

[79] D.V. Taylor, D. Damjanovic, Evidence of domain wall contribution to the dielectric permittivity in PZT thin films at sub-switching fields, J. Appl. Phys. 82 (1997) 1973–1975, https://doi.org/10.1063/1.366006.

[80] L. Mitoseriu, V. Tura, D. Ricinschi, C. Harnagea, Grain size dependence of the Rayleigh coefficients in barium titanate ceramics, Ferroelectrics 240 (2000) 1317–1324, https://doi.org/10.1080/00150190008227952.

[81] N. Bassiri-Gharb, I. Fujii, E. Hong, S. Trolier-Mckinstry, D.V. Taylor, D. Damjanovic, Domain wall contributions to the properties of piezoelectric thin films, J. Electroceram. 19 (2007) 47–65, https://doi.org/10.1007/s10832-007-9001-1.

[82] D. Damjanovic, M. Demartin, Contribution of the irreversible displacement of domain walls to the piezoelectric effect in barium titanate and lead zirconate titanate ceramics, J. Phys. Condens. Matter. 9 (1997) 4943–4953, https://doi.org/10.1088/0953-8984/9/23/018.

[83] P. Bintachitt, S. Jesse, D. Damjanovic, Y. Han, I.M. Reaney, S. Trolier-McKinstry, S.V. Kalinin, Collective dynamics underpins Rayleigh behavior in disordered polycrystalline ferroelectrics, Proc. Natl. Acad. Sci. 107 (2010) 7219–7224, https://doi.org/10.1073/pnas.0913172107.

[84] Y. Wu, J. Zhang, Y. Tan, P. Zheng, Notable grain-size dependence of converse piezoelectric effect in $BaTiO_3$ ceramics, Ceram. Int. 42 (2016) 9815–9820, https://doi.org/10.1016/j.ceramint.2016.03.075.

[85] Z. Cai, X. Wang, W. Hong, B. Luo, Q. Zhao, L. Li, Grain-size–dependent dielectric properties in nanograin ferroelectrics, J. Am. Ceram. Soc. 101 (2018) 5487–5496, https://doi.org/10.1111/jace.15803.

[86] X. Deng, X. Guan, P. Chen, C. Lu, Z. Tan, D. Li, J. Li, X. Wang, L. Li, Ferroelectric properties study for nanocgrain barium titanate ceramics, Thin Solid Films 518 (2010) e75–e77, https://doi.org/10.1016/j.tsf.2010.03.117.

[87] Y. Shi, Y. Pu, Y. Cui, Y. Luo, Enhanced grain size effect on electrical characteristics of fine-grained $BaTiO_3$ ceramics, J. Mater. Sci. Mater. Electron. 28 (2017) 13229–13235, https://doi.org/10.1007/s10854-017-7158-1.

[88] Z.H. Zhang, X.Y. Qi, X.F. Duan, Direct determination of the polarization direction of domains in $BaTiO_3$ single crystal, Appl. Phys. Lett. 89 (2006), 242905, https://doi.org/10.1063/1.2405380.

[89] H. Guo, C. Zhou, X. Ren, X. Tan, Unique single-domain state in a polycrystalline ferroelectric ceramic, Phys. Rev. B 89 (2014), 100104, https://doi.org/10.1103/PhysRevB.89.100104.

[90] A. Bencan, E. Oveisi, S. Hashemizadeh, V.K. Veerapandiyan, T. Hoshina, T. Rojac, M. Deluca, G. Drazic, D. Damjanovic, Atomic scale symmetry and polar nanoclusters in the paraelectric phase of ferroelectric materials, Nat. Commun. 12 (2021) 3509, https://doi.org/10.1038/s41467-021-23600-3.

[91] L. Padurariu, V.-A. Lukacs, G. Stoian, N. Lupu, L.P. Curecheriu, Scale-dependent dielectric properties in $BaZr_{0.05}Ti_{0.95}O_3$ ceramics, Materials (Basel) 13 (2020) 4386, https://doi.org/10.3390/ma13194386.

[92] D.F.K. Hennings, C. Metzmacher, B.S. Schreinemacher, Defect chemistry and microstructure of hydrothermal barium titanate, J. Am. Ceram. Soc. 84 (2001) 179–182, https://doi.org/10.1111/j.1151-2916.2001.tb00627.x.

[93] G. Busca, V. Buscaglia, M. Leoni, P. Nanni, Solid-state and surface spectroscopic characterization of $BaTiO_3$ fine powders, Chem. Mater. 6 (1994) 955–961, https://doi.org/10.1021/cm00043a016.

[94] J. Adam, G. Klein, T. Lehnert, Hydroxyl content of $BaTiO_3$ nanoparticles with varied size, J. Am. Ceram. Soc. 96 (2013) 2987–2993, https://doi.org/10.1111/jace.12404.

[95] D. Hennings, S. Schreinemacher, Characterization of hydrothermal barium titanate, J. Eur. Ceram. Soc. 9 (1992) 41–46, https://doi.org/10.1016/0955-2219(92)90075-O.

[96] Y. Cao, K. Zhu, J. Liu, J. Qiu, Fabrication of $BaTiO_3$ nanoparticles and its formation mechanism using the high temperature mixing method under hydrothermal conditions, Adv. Powder Technol. 25 (2014) 853–858, https://doi.org/10.1016/j.apt.2013.12.012.

[97] K. Hongo, S. Kurata, A. Jomphoak, M. Inada, K. Hayashi, R. Maezono, Stabilization mechanism of the tetragonal structure in a hydrothermally synthesized $BaTiO_3$ nanocrystal, Inorg. Chem. 57 (2018) 5413–5419, https://doi.org/10.1021/acs.inorgchem.8b00381.

[98] C. Pithan, D. Hennings, R. Waser, Progress in the synthesis of nanocrystalline $BaTiO_3$ powders for MLCC, Int. J. Appl. Ceram. Technol. 2 (2005) 1–14, https://doi.org/10.1111/j.1744-7402.2005.02008.x.

[99] X. Zhu, J. Wang, Z. Zhang, J. Zhu, S. Zhou, Z. Liu, N. Ming, Atomic-scale characterization of barium titanate powders formed by the hydrothermal process, J. Am. Ceram. Soc. 91 (2008) 1002–1008, https://doi.org/10.1111/j.1551-2916.2007.02227.x.

[100] M. Shiojiri, T. Isshiki, H. Saijo, M. Tsujikura, A. Nakada, Y. Nakano, M. Ikeda, T. Nomura, High-resolution electron microscopy study of domain boundaries and dislocation loops in $BaTiO_3$ crystals, Phys. Status Solidi 129 (1992) 353–362, https://doi.org/10.1002/pssa.2211290206.

[101] T. Suzuki, M. Ueno, Y. Nishi, M. Fujimoto, Dislocation loop formation in nonstoichiometric $(Ba,Ca)TiO_3$ and $BaTiO_3$ ceramics, J. Am. Ceram. Soc. 84 (2001) 200–206, https://doi.org/10.1111/j.1151-2916.2001.tb00631.x.

[102] D. Schrade, R. Mueller, D. Gross, T. Utschig, V.Y. Shur, D.C. Lupascu, Interaction of domain walls with defects in ferroelectric materials, Mech. Mater. 39 (2007) 161–174, https://doi.org/10.1016/J.MECHMAT.2006.04.002.

[103] Z. Wang, M. Saito, K.P. McKenna, Y. Ikuhara, Polymorphism of dislocation core structures at the atomic scale, Nat. Commun. 5 (2014) 3239, https://doi.org/10.1038/ncomms4239.

[104] Y. Liu, Y.-L. Tang, Y.-L. Zhu, W.-Y. Wang, X.-L. Ma, Spatial coupling of ferroelectric domain walls and crystallographic defects in the $PbTiO_3$ films, Adv. Mater. Interfaces 3 (2016), 1600342, https://doi.org/10.1002/admi.201600342.

[105] M.-W. Chu, I. Szafraniak, R. Scholz, C. Harnagea, D. Hesse, M. Alexe, U. Gösele, Impact of misfit dislocations on the polarization instability of epitaxial nanostructured ferroelectric perovskites, Nat. Mater. 3 (2004) 87–90, https://doi.org/10.1038/nmat1057.

[106] R.C. Bradt, G.S. Ansell, Dislocations and 90° domains in barium titanate, J. Appl. Phys. 38 (2004) 5407, https://doi.org/10.1063/1.1709334.

[107] T. Kiguchi, K. Aoyagi, Y. Ehara, H. Funakubo, T. Yamada, N. Usami, T.J. Konno, Configuration and local elastic interaction of ferroelectric domains and misfit dislocation in $PbTiO_3/SrTiO_3$ epitaxial thin films, Sci. Technol. Adv. Mater. 12 (2011), 034413, https://doi.org/10.1088/1468-6996/12/3/034413.

[108] S.Y. Hu, Y.L. Li, L.Q. Chen, Effect of interfacial dislocations on ferroelectric phase stability and domain morphology in a thin film—A phase-field model, J. Appl. Phys. 94 (2003) 2542, https://doi.org/10.1063/1.1590416.

[109] A. Pramanick, A.D. Prewitt, J.S. Forrester, J.L. Jones, Domains, domain walls and defects in perovskite ferroelectric oxides: a review of present understanding and recent contributions, Crit. Rev. Solid State Mater. Sci. 37 (2012) 243–275, https://doi.org/10.1080/10408436.2012.686891. Https://Doi.Org/10.1080/10408436.2012.686891.

[110] M. Höfling, X. Zhou, L.M. Riemer, E. Bruder, B. Liu, L. Zhou, P.B. Groszewicz, F. Zhuo, B.-X. Xu, K. Durst, X. Tan, D. Damjanovic, J. Koruza, J. Rödel, Control of polarization in bulk ferroelectrics by mechanical dislocation imprint, Science (80-.) 372 (2021) 961–964, https://doi.org/10.1126/SCIENCE.ABE3810.